Platinum Group Element (PGE) Mineralization Associated with Fe-Ti-V Deposit, Rio Jacaré Intrusion, Bahia State, Brazil

Robert Anderson Campbell

Submitted in Partial Fulfillment of the Requirements

For the Degree of Bachelor of Earth Sciences, Honours

Department of Earth Sciences

Dalhousie University, Halifax Nova Scotia

April, 2012

Distribution License

DalSpace requires agreement to this non-exclusive distribution license before your item can appear on DalSpace.

NON-EXCLUSIVE DISTRIBUTION LICENSE

You (the author(s) or copyright owner) grant to Dalhousie University the non-exclusive right to reproduce and distribute your submission worldwide in any medium.

You agree that Dalhousie University may, without changing the content, reformat the submission for the purpose of preservation.

You also agree that Dalhousie University may keep more than one copy of this submission for purposes of security, back-up and preservation.

You agree that the submission is your original work, and that you have the right to grant the rights contained in this license. You also agree that your submission does not, to the best of your knowledge, infringe upon anyone's copyright.

If the submission contains material for which you do not hold copyright, you agree that you have obtained the unrestricted permission of the copyright owner to grant Dalhousie University the rights required by this license, and that such third-party owned material is clearly identified and acknowledged within the text or content of the submission.

If the submission is based upon work that has been sponsored or supported by an agency or organization other than Dalhousie University, you assert that you have fulfilled any right of review or other obligations required by such contract or agreement.

Dalhousie University will clearly identify your name(s) as the author(s) or owner(s) of the submission, and will not make any alteration to the content of the files that you have submitted.

If you have questions regarding this license please contact the repository manager at dalspace@dal.ca.

Grant the distribution license by signing and dating below.

_____ _____

Name of signatory Date

Abstract

The Rio Jacaré intrusion is located in north eastern Brazil, inside the state of Bahia. Primarily explored for its abundant titaniferous-vanadium rich magnetite occurrences, the intrusion also contains elevated levels of platinum (Pt) and palladium (Pd) ("Gulcari A" magnetite deposit researched in this study). The layered mafic intrusion is composed predominantly of gabbroic rocks, containing rhythmic cycles of magnetite-pyroxenite-gabbro-anorthosite. Fine grained, magnetite-rich rocks initiate the cycle followed by pyroxenite, generally capped by coarser gabbro or thin lenses of anorthosite. Unlike the common association of Platinum Group Mineral (PGM) mineralization with chromite layers within Layered Mafic Intrusions (LMI), the Rio Jacaré is a rare example of PGM mineralization within magnetite lenses. Processes regarding the enrichment of PGM mineralization remain unclear. A detailed mineralogical investigation was conducted on PGM mineralization within the main magnetite deposit, Gulcari A, aiming to understand the nature of PGM crystallization.

Thirteen samples with elevated Platinum Group Element (PGE) concentrations (1050-5026 ppm Pt, 25-1106 ppm Pd) were selected for this study. Reflected light microscopy and Energy Dispersive Spectroscopy (EDS) analyses were used for mineral identification. The chemical composition of PGMs was determined using electron microprobe (EMP) analyses. The ore consists of a magnetite-ilmenite aggregate, annealed and re-crystallized during metamorphism. Sulphide phases fill the interstitial space and are associated with gangue minerals. The most common Pt-phases found in these slides are: sperrylite ($PtAs_2$), tetraferroplatinum (PtFe), niggliite (PtSn), PtNiFe, PtNi, PtSbSnNiCoS, and PtAsFeNi. The most common Pd-phases found are; PdPtSnCu, PdBiTe, PdBiSb, and PdSn. Pt-phases are found as inclusions within magnetite, ilmenite and occasionally late-forming gangue minerals. Often, PGMs form at the boundary between early magnetite-ilmenite grains and interstitial gangue minerals. Additionally, sperrylite grains have been found as partial inclusions within larger arsenide minerals. Pd-phases are found as inclusions within late gangue minerals, partial inclusions within arsenides, growths along grain boundaries between gangue minerals and primary magnetite-ilmenite grains, and as small subhedral grains within interstitial space. Overall, PGM mineralization varies from small 2 μm, to larger 100 μm anhedral grains. The average grain size of PGM mineralization is between 2-10 μm.

Our results suggest two different events responsible for the entrainment and remobilization of PGe mineralization. In our study we tested both the proposed earlier mechanism of exsolution of PGMs from late sulphide phases, and remobilization of PGE's by late hydrothermal fluids.

Table of Contents

Table of Figures

Table of Tables

Table of Abbreviations

Mineral Name	*Chemical Formula*	*Abbreviation*
Magnetite	Fe_3O_4	Mt
Ilmenite	$FeTiO_3$	Ilm
Chalcopyrite	$CuFeS_2$	Cpy
Pyrite	FeS_2	Py
Galena	PbS	Ga
Sphalerite	ZnS	Sph
Chalcocite	Cu_2S	Ch
Bravoite	$(Fe,Ni,Co)S_2$	Br
Cobaltite	CoAsS	Cb
Alloclasite	(Co,Fe)AsS	Al
Pentlandite	$(Fe,Ni)_9S_8$	Pl
Orcelite	Ni_5As_2	Or
Krutovite	$NiAs_2$	Kt
Dienerite	Ni_3As	Dt
Sperrylite	$PtAs_2$	Spy
Tetraferroplatinum	PtFe	Tp
Niggliite	PtSn	Nt
Paolovite	Pd_2Sn	Pv

Acknowledgements

I would like to give a special thank you to my supervisor, Dr. Yana Fedortchouk. I now have a healthy appreciation for the time, effort and patience needed, to assist a student in his or hers honour's project. I would also like to extend my appreciation to Largo Resources Ltd. Largo, provided an interesting problem to tackle, and financially supported the technical work performed. In particular Mr. Israel Nonato, Senior Geologist, was a real asset while visiting the Maracas project. He provided the field experience necessary to understand the big picture. Also I would like to thank Dan MacDonald and Bob Barnett who provided a wealth of microprobe knowledge and experience, which proved critical to my understanding of the geological system. Finally, I'd like to thank my father Mr. Robert Anderson Campbell. He provided the project, facilitated the funding, and most importantly made himself available for questioning. Thanks to those above who made this a fun and enjoyable experience

Chapter 1: General Statement

The Rio Jacaré intrusion, located in Bahia, north eastern Brazil, has largely been explored for its vanadium rich, titaniferous magnetite layers. In addition to anomalous Fe-Ti-V occurrences are significant concentrations of platinum and palladium. More extensive research into mineralization associated with platinum group elements (PGE) is needed to determine whether there is a viable economic deposit present.

The Rio Jacaré intrusion was initially mapped in the 1970's and 1980's by Companhia Baiana Pesquisa Mineral (CBPM), a Bahia state owned exploration company (Sá et al. 2005). CPBM found that the Rio Jacaré intrusion is enriched in vanadium along with elevated levels of both Pt and Pd. Mineralization in the Rio Jacaré is hosted within vanadium rich, titaniferous magnetite layers, a defining characteristic of this deposit. This is intriguing because the Platinum Group Mineral (PGM) horizons are different from those in the larger well known layered mafic intrusions (e.g. the Bushveld). In the Bushveld, chromite layers compartmentalize PGM zones while in the Rio Jacaré PGMs have been concentrated in massive magnetite horizons.

The Maracas property owned by Largo Resources Ltd. of Toronto (Largo) is being developed primarily with the goal of extracting vanadium. Elevated levels of PGE's within magnetite layers can be refined and processed if proven economic. This thesis looks to understand the geological and geochemical process that allowed for the entrainment and enrichment of PGMs.

1.1 Geologic Setting

The Rio Jacaré intrusion lies within the São Francisco craton (2.5-2.0 Ga) (Fig, 1.1). The São Francisco craton is composed of a number of blocks and belts including the Jequié (2.9-2.6 Ga) to the east, and Gavião (3.4-3.0 Ga) to the west, and in between, the younger mobile belt named the Contendas-Mirante supercrustal sequence (2.0 Ga) (Sá et al. 2005). Wedged between the Contendas-Mirante and Jequié is the Rio Jacaré intrusion (2.8-2.47 Ga), a linear, sheet-like structure that can be traced over 70 km with an average width of 1.2 km.

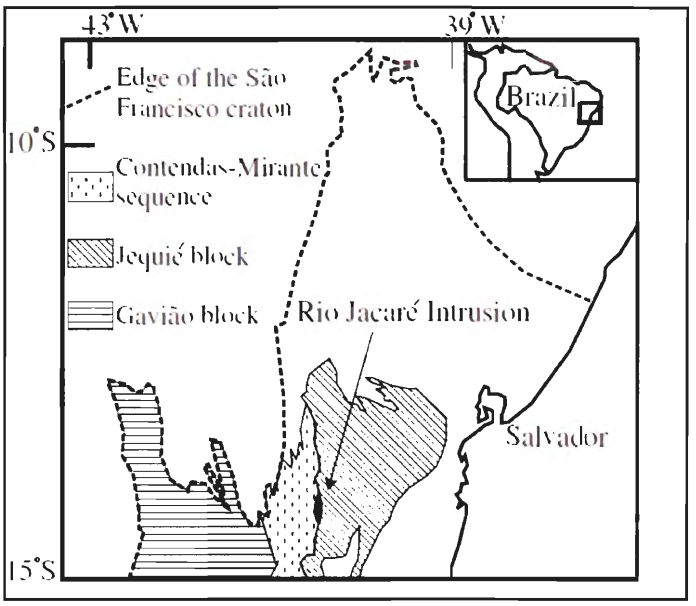

Figure 1.1: Map showing the Rio Jacaré in relation to the older tectonic units on each side (Sá et al., 2005).

The Gavião block is composed of Tonalite-Trondhjemite Granodiorites (TTG's) (Sá et al. 2005). The younger Jequié block is composed of plagioclase (enderbrite)/orthopyroxene (charnokite) granites along with granulite facies metamorphic rocks. The Contendas-Mirante is composed of a deformed sequence of Archean basal volcanic units followed by a Paleoproterozic unit of flysh and metavolcanic rocks (Sá et al. 2005). Metamorphism is present in the Jequié, Contendas-Mirante and the Rio Jacaré intrusion. The Rio Jacaré Intrusion consists of mafic to ultramafic intrusive rocks mainly of gabbroic composition further discussed in Chapter 2.

Deformation and metamorphism present in both the Contendas-Mirante sequence and the Rio Jacaré Intrusion occurred during the Trans-Amazonian Orogeny (2.14-1.94 Ga), in which both Gavião and Jequié blocks collided with the Contendas-Mirante sequence and the Rio Jacaré

intrusion. This formed a portion of the Contendas-Jacobina lineament (Hennessey, 2006). Geologically, this has been interpreted as the opening and closing of a rift system. The basal metavolcanic rocks of the Contendas-Mirante sequence and the primitive mafic to ultramafic intrusive rocks of the Rio Jacaré intrusion are consistent with the remnants of the structures created by the opening and closing of the rift. In addition, the timing of the Trans-Amazonian Orogeny correlates with the age of intrusive pegmatitic veins found in the Rio Jacaré.

PGM mineralization is speculated to be magmatic in origin. However, metamorphism may have facilitated re-crystallization and remobilization. Both models of PGM mineralization will be considered.

1.2 Samples and Locations

The samples for this thesis were taken from Largo's Maracas project. Largo has provided hand samples, thin sections and analytical results from each lithology associated with the layered mafic intrusion. Hand samples were collected by Mr. Israel Nonato, senior exploration geologist for Largo. Global positioning system (GPS) coordinates have been taken for each hand sample. The thin section suite consists of thirteen sections with high PGE occurrences. Geographic coordinates along with drill hole depths are provided for each thin section sample (Table 1.).

Table 1.1: High PGE samples received from Largo Resources, Pt/Pd grades determined by geochemical assay.

HOLE-ID	*FROM*	*TO*	*Pt (ppb)*	*Pd (ppb)*
FGA-03	**42**	**43**	**1839**	**1106**
FGA-04	**47**	**47.75**	**2008**	**179**
FGA-07	**52**	**52.54**	**1299**	**82**
FGA-14	**22.4**	**23**	**1803**	**103**
FGA-17	**82**	**83**	**1790**	**182**
FGA-20	**52**	**53**	**5026**	**92**
FGA-20	**53**	**54**	**3526**	**154**
FGA-23	**49**	**50**	**1308**	**248**
FGA-43	**104**	**105**	**4235**	**105**
FGA 58	**140.20**	**141.00**	**4998**	**407**
FGA 61	**76.00**	**77.00**	**1050**	**25**
FGA 69	**45.00**	**46.00**	**2056**	**35**
FGA 80	**23.00**	**24.00**	**3927**	**208**

1.3 Previous Work

CBPM was the first company to discover and explore for vanadium on the Maracas property. Exploration programs carried out by CBPM occurred from the late 1970's through to 1980's. They included sampling, mapping and diamond drilling. In 1984, Odebrecht, a private Brazilian engineering firm entered a joint venture with CBPM and began drilling on the Maracas property. From 1981 to 1987, 53 drill holes and 21 trenches were completed on the Gulcari "A" deposit, the main showing within the Maracas project (Hennessey, 2006). In the 1990's, Odebrecht obtained 90% of CBPM and created another 50/50 joint venture with CAEMI. CAEMI is presently a wholly-owned subsidiary of Vale, the world's largest iron-ore company. CAEMI was brought on to add expertise in developing the Maracas project into a producing mine. In 2006 Largo Resources Ltd. optioned the Maracas property from Odebrecht and CAEMI (Vale). To date, the most extensive research done on Maracas' PGE potential was published by Sá et al. (2005).

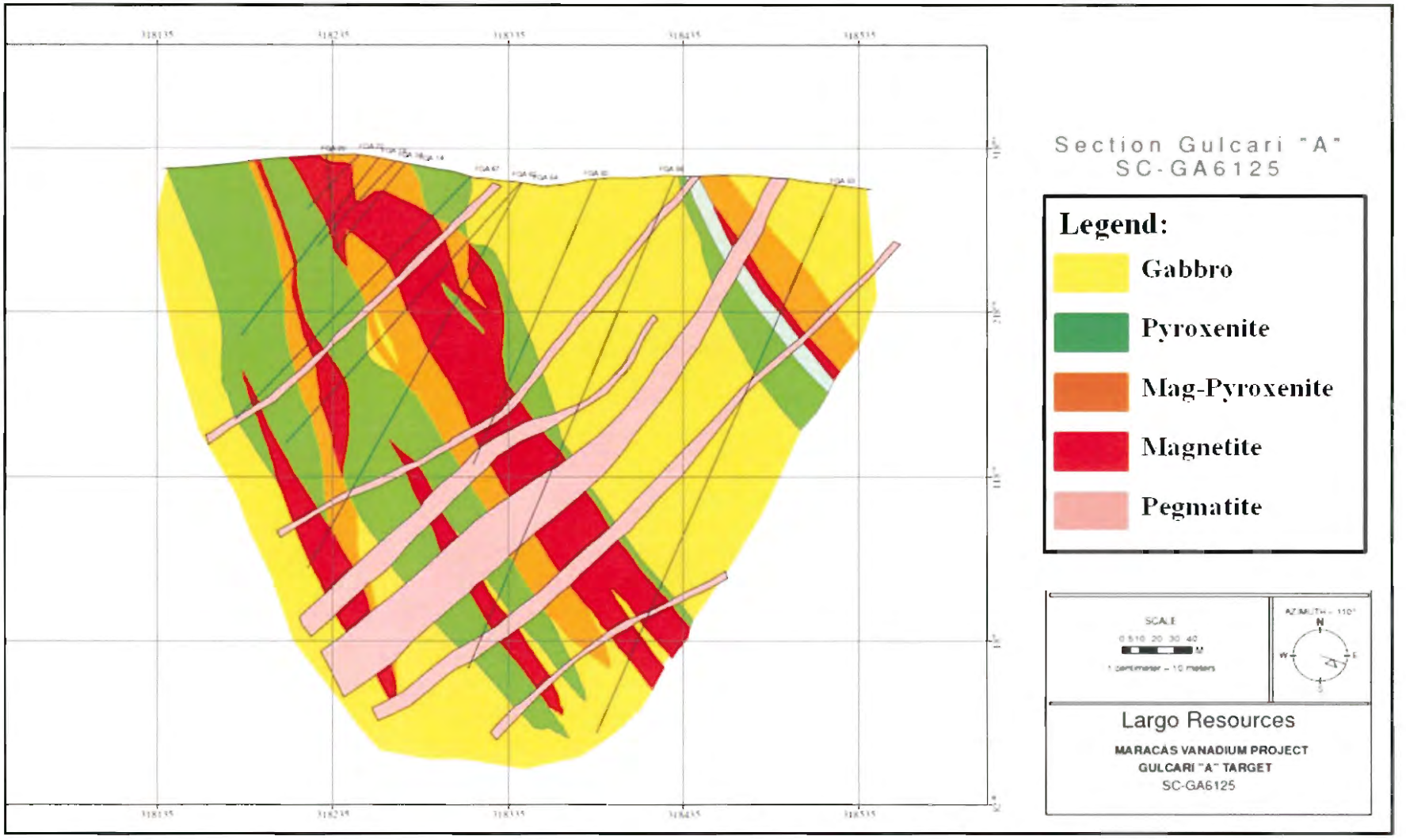

Figure 1.2 Sample FGA20 (52-53), FGA20 (53-54) and FGA04 are located in section 6125. The cross section is oriented 290°. The thin blue lens represents an anorthosite layer. Modified from (Largo)

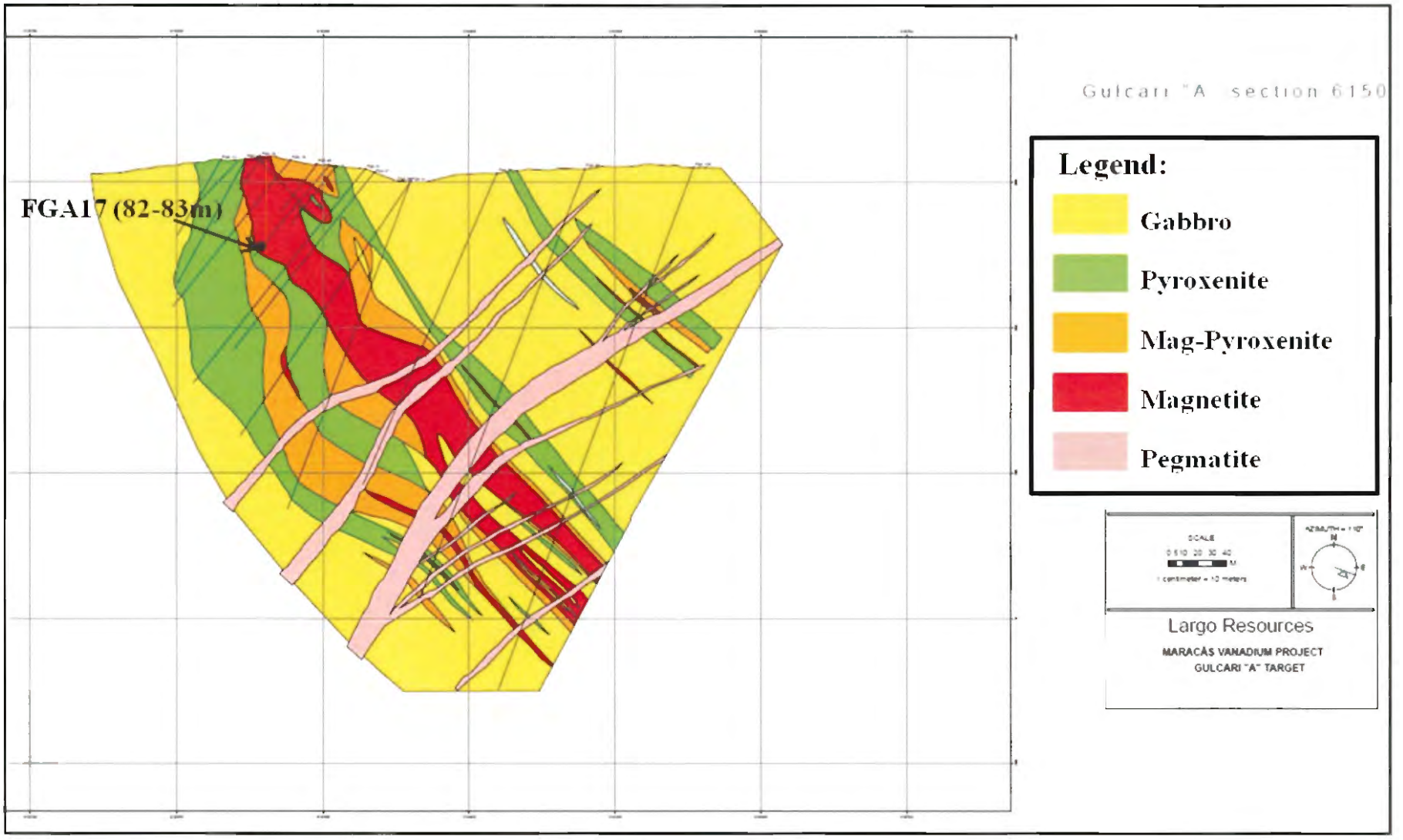

Figure 1.3 Sample FGA17 is found within the Gulcari "A" pod in section 6150. The cross section is oriented at 290°. The thin blue lens represents an anorthosite layer. Modified from (Largo).

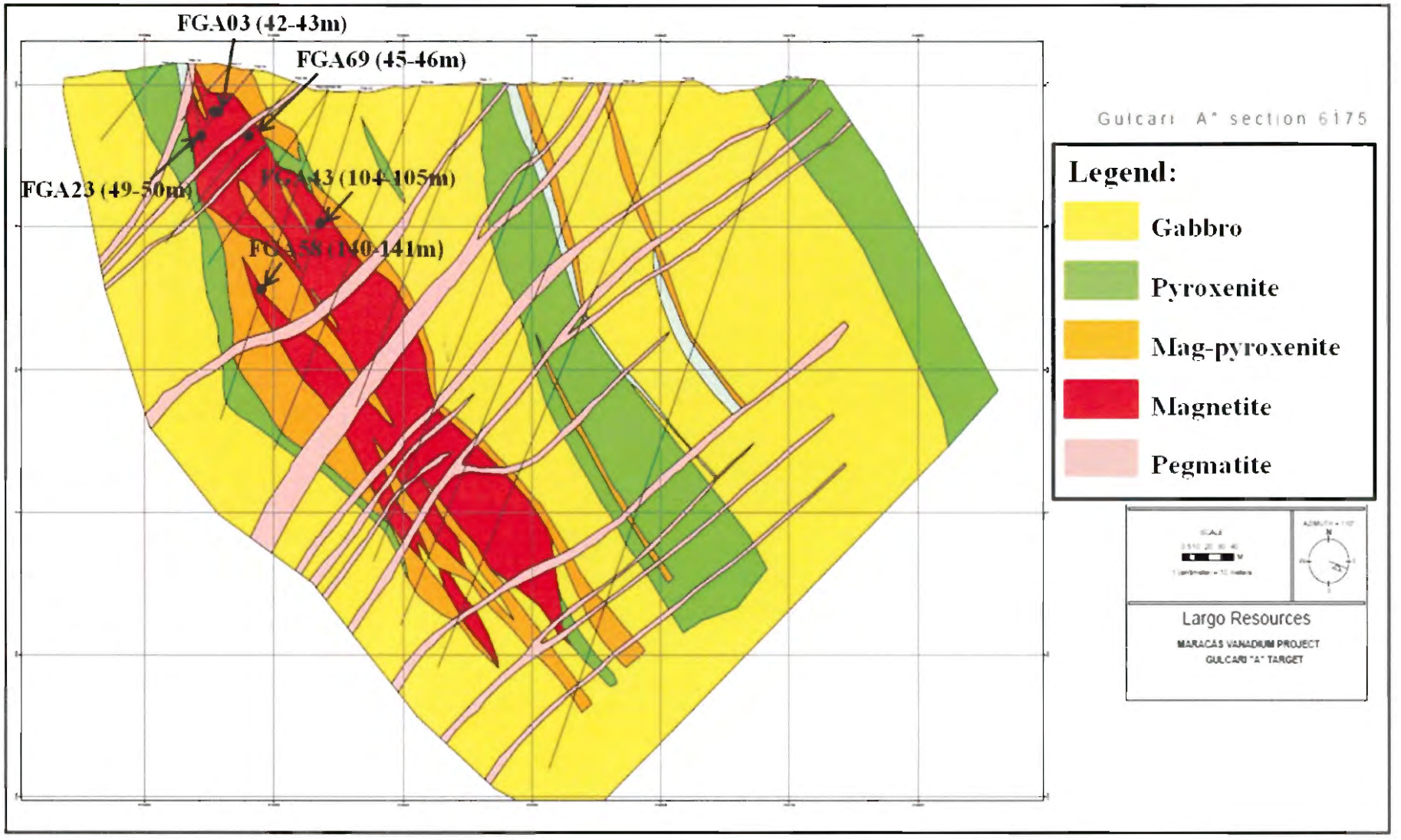

Figure 1.4 Samples FGA23, FGA03, FGA43 and FGA58 are found in section 6175. The cross section is oriented at 290°. The thin blue lenses represent anorthosite Modified from (Largo).

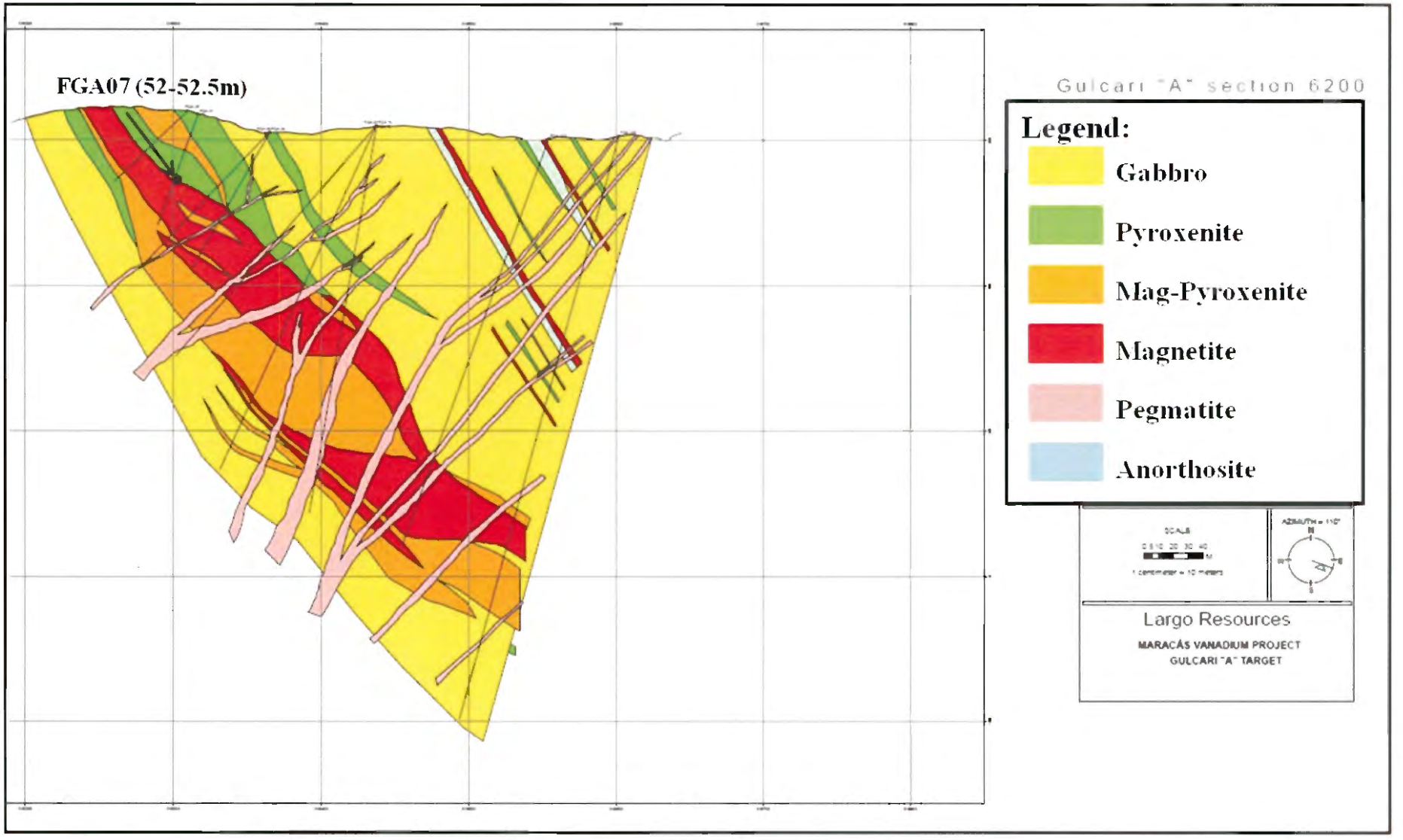

Figure 1.5 Sample FGA07 is located in section 6200 of the Gulcari "A" magnetite pod. The cross section is oriented at 290° Modified from (Largo)

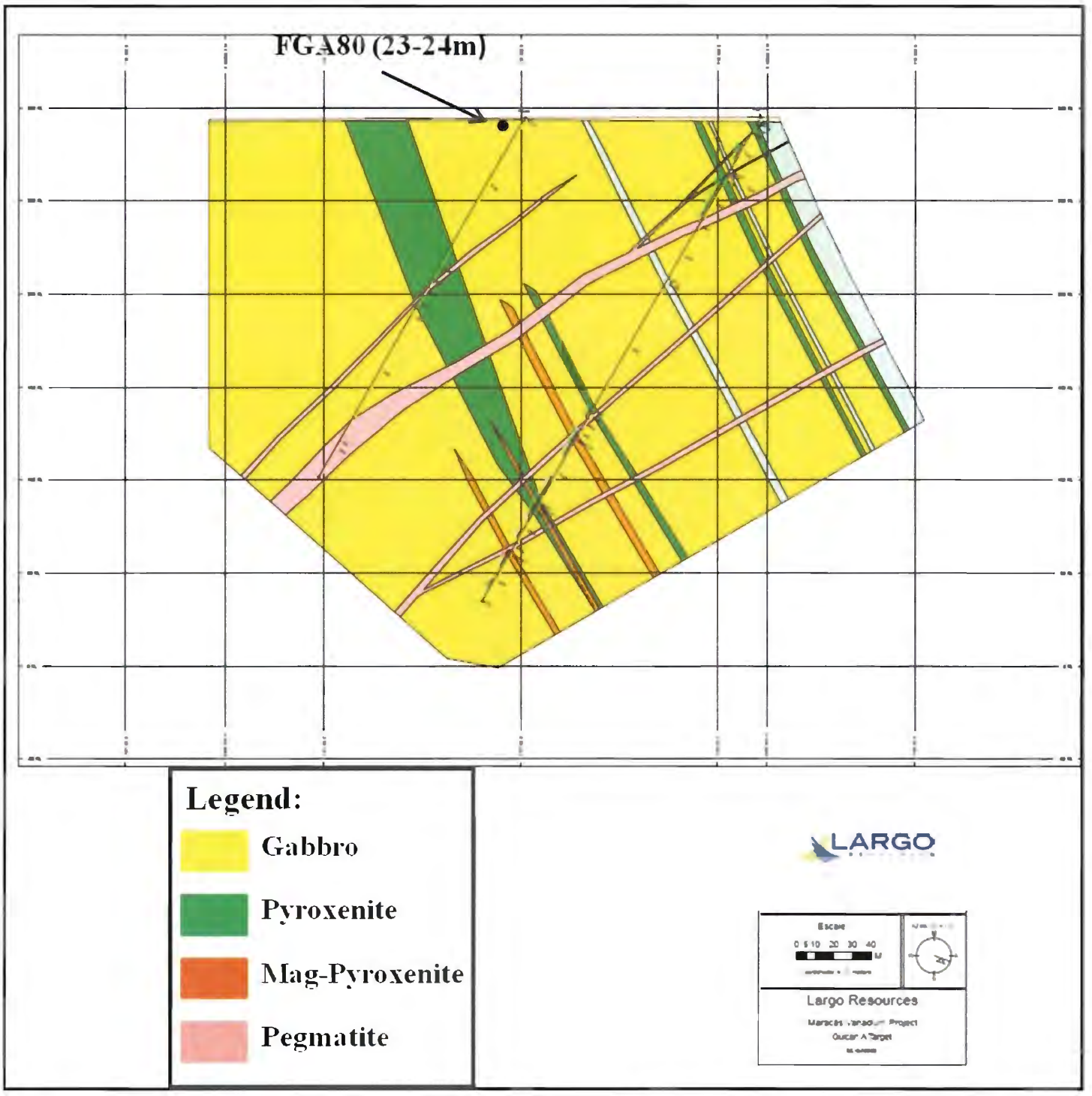

Figure 1.6 Sample FGA80 is located in section 6000, the cross section is oriented at 290°. The thin blue lenses represent anorthosite layers. Modified from (Largo) *(Samples FGA14 & FGA61 were drilled at locations were a cross section is unavailable)*

1.4 Objectives

The main objective of this study is to better understand the formation and enrichment of PGMs at the Maracas property within the Rio Jacaré intrusion. Using electron microprobe analyses, all PGE bearing phases present in the Gulcari "A" deposit were identified. In addition, all ore minerals were identified along with their relationships to PGMs and associated lithologies. A thorough understanding of the textures and minerals present allows us to develop a crystallization sequence for all of the ore minerals present. A final goal is to determine the origin of PGE mineralization.

1.5 Methods

1.5.1 EDS and WDS Analyses

The primary method of analysing platinum group minerals in this study is done through use of the electron microprobe. Wave Dispersive Spectroscopy (WDS) and Electron Dispersive Spectroscopy (EDS) were used to analyse the phases of PGMs present. Backscatter Electron (BSE) images were used to identify PGMs and other ore minerals present. Of the minerals present, there is a high contrast between the atomic weight of ore minerals and gangue minerals. Gangue minerals appear very dark in BSE images, due to their low atomic weight. Magnetite and ilmenite are light gray, while PGMs are white because of their high atomic weight. Heavy sulphides and arsenides also occur as white grains, but are distinguished when analysed. Using reflected light microscopy, modal abundances for each sample were determined. Reflected light is useful for determining textures present within the sample. By compiling detailed analyses of each sample, any correlation between PGM abundance and lithology, depth, mineralogy, etc can be interpreted.

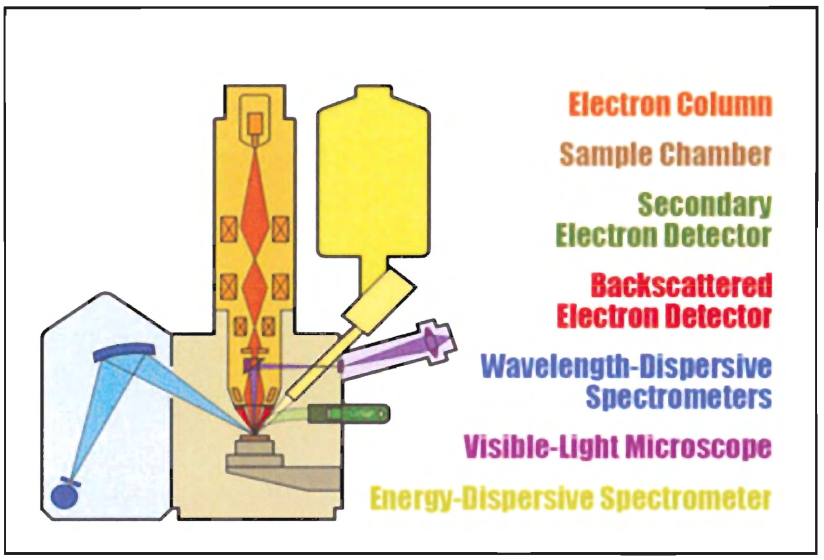

Figure 1.2 Working components of the electron microprobe.

Energy dispersive spectroscopy measures x-ray energy given off by individual minerals. After the electrons are sorted through a filter, a computer determines which elements are present within the mineral based on the intensity of x-rays emitted. Energy is detected by a lithium-drifted silicon or high purity germanium crystal (Freil, 1998). As the energy enters the crystal it produces a charge pulse that is proportional to the x-ray energy. Advantages of EDS are: no moving parts, entire spectrum collected at once, high quantum efficiency and high collection efficiency. Disadvantages are peak overlap and spectral artefacts.

Wavelength Dispersive Spectroscopy measures characteristic wavelengths to identify elements present. An analyzing crystal positioned in front of the x-ray detector screens out everything but the desired wavelength (Freil, 1998). Using Bragg's law:

(1.1)

the wavelength of given element can be determined. Spectrometers analyse the angle of incoming x-rays to satisfy Bragg's Law. High spatial resolution allows for both quantitative

analyses, along with analyses of chemical zoning within a mineral (Goodge, 2011). WDS also provides improved peak resolution of elements when compared to EDS. Disadvantages of WDS are that it is expensive and it is unable to analyse elements below the atomic number five. Important elements such as H, Li, and Be cannot be analysed (Goodge, 2011). Additionally, WDS cannot determine different valence states of elements (e.g. Fe^{2+}, Fe^{3+}).

Both methods of EMP analysis were applied in the study of ore minerals from the Rio Jacaré intrusion. Samples were cleaned with an alcohol solution and then carbon coated. EDS was used to identify the composition of small grains (> 5μm). Analyses of grains larger than 5μm were done using WDS with a JEOL microprobe (Department of Earth Sciences, Dalhousie University), using a voltage of 15 kV, amperage of 12μA, and a beam size of 1μm. Standards used were calibrated once a week by Mr. Dan Macdonald, and peak searches were performed during the morning prior to analyses.

A twenty-four element suite was used when analysing the PGE enriched thins sections. Pure metal standards were used for Au, Ir, Os, Pt, Ru, Rh, Ag, V, and Cr. $FeTe_2$ was used for Te, Bi_2Se_3 for Bi, arsenopyrite for As, sanadine for Al, $PdBi_2$ for Pd, (kakanui) kaersutite for Mg, pyrrhotite for Fe & S, cinnabar for Hg, cobaltite for Co, crocoite for Pb, stibnite for Sb, pentlandite for Ni, chalcopyrite for Cu, and rutile for Ti.

1.5.2 (AA) Spectroscopy and ICP-MS

Atomic Adsorption (AA) spectroscopy was developed in the 1950's, to study whole rock geochemistry, and is used to determine the concentration of over 70 different elements. The process works by spraying a solution (of unknown concentration) in a flame or graphite furnace (Winter, 2010). A beam of light, of known wavelength, is passed through the furnace and the reduction in light intensity (absorption) is measured.

Inductively Coupled Plasma Mass Spectrometry (ICP-MS) was introduced in the 1970's and can analyse a sample for 60 elements within minutes (Winter, 2010). Samples are put into solution, mixed with argon gas, and then aspirated into a tiny radio frequency generator to create plasma. Atoms are consequently excited, and the emission of energy is isolated by a diffraction grating, which spacing is characteristic of an individual element. A computer takes the raw data and calculates the concentration of each element.

1.5.3 Trace Element Geochemistry

Geochemical analyses of whole rock were done by ACME Analytical Laboratories LTD. in Vancouver and SGS GEOSOL Laboratories LTD. in Belo Horizonte, Brazil. Sixty samples were sent to ACME, then crushed and pulverized to 150 mesh, followed by major and trace element analysis. Fire assay fusion was done on Pt, Pd, and Au followed by ICP-MS. A separate suite of twenty-four samples was sent to GEOSOL, samples were initially crushed to 2mm, pulverised and put through 150 mesh. Platinum and palladium were put through a 50g fire assay followed by atomic absorption (AA) spectroscopy.

Trace element geochemistry was used to better understand the crystallization of the intrusion. Geochemical analyses can also provide an indication of fluids, if present. Spyder diagrams provide a visual representation of geochemical variation with respect to the standard chrondrite. All chrondrite values were taken from McDonough & Suns, (1995) (www.earthref.org). Comparison to chrondrite values give an indication of relative enrichment compared to primitive mantle concentrations. Data from pegmatite, gabbro, pyroxenite, magnetite-pyroxenite and magnetite lithologies were each initially plotted individually to see if there was any variation.

Chapter 2: Layered Mafic Intrusions

There are multiple examples of layered mafic intrusions (LMI) across the globe. The largest, most famous layered intrusions are: the Bushveld (South Africa), Stillwater (Montana), Duluth (Minnesota), Great Dyke (Zimbabwe) and Skaergaard (Greenland). These intrusions are characterized by compositional layering, present throughout the igneous complex. During the Precambrian, a high geothermal gradient caused large amounts of mantle melting which allowed layered intrusions to be emplaced within continental crust (Winter, 2010). Many, but not all, layered intrusions formed during the Precambrian including the Stillwater, Duluth, Bushveld, and Rio Jacaré. The Skaergaard intrusion is an example of an LMI that formed in the Eocene. There are two stipulations necessary to form a layered intrusion. First, a critical intrusion thickness of 400-500 m is needed to allow for differentiation, forming the layering. Secondly there needs to be a large quantity of magma. Cooling periods for these intrusions vary with size, intrusions can take thousands to millions of years too cool (Winter, 2010). The general shape of layered intrusions is a funnel or a lopolith. The difference between a funnel and lopolith is that a funnel cross cuts the strata while a lopolith is conformable with the strata. LMI's are found in intracratonic settings, usually associated with continental rifting and large igneous provinces (LIP). Often LMI's form in association with coeval continental flood basalts.

Table 2.1 Large layered mafic intrusions of the world. Modified from (Winter, 2010).

Name	Age	Location	Area (km2)
Bushveld	~2.0 Ga	South Africa	66,000
Dufek	~170 Ma	Antarctica	50,000
Duluth	~1.2 Ga	Minnesota	4,700
Stillwater	2.7 Ga	Montana	4,400
Muskox	1.095-1.155 Ga	Northwest Territories, Canada	3,500
Rio Jacaré	2.47 Ga	Brazil	84
Great Dike	2.575 Ga	Zimbabwe	3,300
Skaergaard	55 Ma	Eastern Greenland	100

2.1 Igneous Layering

Igneous layering defines a layered mafic intrusion. Processes such as partial melting and fractional crystallization can produce rhythmic layers within an LMI. Layers can be defined by a change in rock type, mineral composition (modal composition changes), change in chemical composition of minerals (cryptic), or change in texture. Layering can be homogenous (uniform) or heterogeneous (non-uniform). Graded layers (i.e., fining upwards sequence) are an example of a non-uniform layering. Rhythmic layering is defined by the repetition of a sequence of layers. Macrorhythmic layering describes a sequence of layers with a thickness of several meters while microrhythmic layering is used for sequences on the order of a few centimetres (Winter, 2010). Moving from the source of the intrusion upwards, magmatic fractionation can produce chemical changes in layering. In the Bushveld, the lower portion of the intrusion is dominated by ultramafic to mafic rocks, composed predominantly of compatible elements (e.g., Mg, Fe, Cr,

Si). Travelling stratigraphically upwards the magma becomes increasingly enriched in incompatibles and becomes more felsic.

2.2 Crystallization in LMI

Gravity settling is the most universally accepted mechanism for magmatic differentiation within a LMI. Crystal settling follows the laws of Newtonian fluids and heavier crystals fall out of suspension. Rhythmic layering can be explained by a single session of crystal settling followed by large-scale convective overturn (Winter, 2010). Overturn removes late liquid from the system and recycles (homogenizes) the magma and then another pulse repeats the process.

In situ crystallization requires the nucleation of crystals in a thin, stagnant layer along the boundary of the magma chamber (Winter, 2010). This method of crystallization was proposed to account for inconsistencies in the gravity settling model. A boundary layer forms in a stagnant zone and separates the melt from the thin layer of growing crystals. This impermeable membrane prevents minerals like plagioclase from floating and olivine from sinking out of one layer and into another. Layering forms through the process of double-diffusive convection. Contrasting gradients, thermal density and vertical compositional density, for example, create a series of convecting layers.

2.3 PGE Mineralization in LMI

2.3.1 Orthomagmatic Model

Platinum group minerals can be found in a selection of rock types depending on the geochemistry of the layered intrusion. Typically mineralization is concentrated in "reefs" or thin horizons within the lower ultramafic section of the intrusion. PGE mineralization is typically associated with chromite horizons, e.g. in the Bushveld, Great Dyke, Stillwater, and Kami. These are a few examples of PGE mineralization related to stratiform chromite deposits.

In the Rio Jacaré intrusion, PGE mineralization is concentrated within magnetite pods. PGE's (platinum, palladium, ruthenium, rhodium, osmium, and iridium) are highly siderophile and have a strong affinity for native iron. PGE's also strongly partition into sulphide melts. Platinum group minerals are likely derived from mantle melts that are sulphur-poor and PGE-enriched (Maier, 2005). Extensive degrees of partial melting are required to allow PGE's to separate from the mantle and become incorporated into the melt. Further evidence of large degrees of partial melting is found in the Mg-rich signature of important PGE deposits. Both chromite and magnetite help to precipitate PGE's by causing sulphide, and in the case of the Rio Jacaré, arsenide saturation. The crystallization of these iron-rich minerals lowers the oxygen fugacity allowing for sulphur saturation (Maier, 2005).

Liquid immiscibility occurs when a silicate magma becomes sulphide-saturated (Winter, 2010). Less than 1% of sulphur is required to adequately saturate a siliceous magma. Once saturated, the magma separates into two immiscible fluids, one siliceous, the other sulphide rich. Sulphur along with strongly chalcophile (Cu, Ni, Pb, etc) and siderophile (PGE's) elements form small, round, immiscible sulphide droplets. The R factor indicates a ratio of silicate/sulphide liquid mass (Robb, 2005). This ratio effectively records the extent to which the immiscible sulphide melt interacts with its corresponding silicate magma (Robb, 2005). Sulphide melt separates and is immiscible with the rest of the melt. As dense sulphide droplets fall to the bottom of the magma chamber they strongly partition chalcophile and siderophile elements such as base metals and PGE's (Maier, 2005). A sulphide globule's ability to interact with a large volume of silicate magma increases its opportunity to scavenge PGE's. As the magma rises, sulphides may be reworked into the melt. Pressure is reduced during ascent, which allows for

more sulphide saturation. This process accommodates sulphide entrainment. Zones of mineralization are usually tens of meters wide and concentrated in ultramafic rock suites.

2.3.2 Hydrothermal model

Platinum and palladium can also be transported through chlorine-rich fluids. Pt forms the following chlorine complex:

$$Pt^{2+}_{(aq)} + 4Cl^{-}_{(aq)} \longrightarrow PtCl_4^{2-}{}_{(aq)} \qquad (2.1)$$

Chlorine complexation enables large stability constants, allowing for high Pt solubility. These complexes also allow for increased stability of Pt and Pd over a wide range of pH and Cl^- concentration conditions (Hanley, 2005). Cl^- rich fluids exsolve from the cumulate pile and migrate stratigraphically upwards, due to oversaturation and crystal compaction, into a hotter intercumulus liquid. The Cl^- rich fluid dissolves in the undersaturated magma reducing Pt and Pd solubility, causing the metals to precipitate and form enriched mineralized horizons (Hanley, 2005). The bisulphide ion (HS^-) can also be important in PGE transport, HS^- behaves like Cl^- at neutral pH and low temperatures. Mineralization due to the presence of HS^- will be found in the form of platinum and palladium sulphides. This process has been demonstrated in both the Bushveld and Stillwater layered mafic intrusions.

2.4 Rio Jacaré Intrusion

The Rio Jacaré intrusion has a length of 70km generally striking north-south and an average width of 1.2km (Sá et al., 2005). The dip of the intrusion, along with the layering is 70° E. The contacts between the Contendas-Mirante supercrustal sequence and the Jequié blocks are faulted. The intrusion is composed predominantly of gabbroic rocks, and locally there are horizons of pyroxenite, anorthosite and magnetite (lenses). Whole-rock dating of the intrusion using Pb/Pb provides an age of 2.47 Ga ± 72 Ma (Sá et al., 2005) and Sm/Nd an age of 2.8 Ga ± 68 Ma (Brito

et al., 2001). Discrepancies around the true age of the intrusion have yet to be resolved. Around 1.94 Ga ± 54 Ma, the Rio Jacaré was intruded by granitic pegmatite veins (Fig. 2.1).

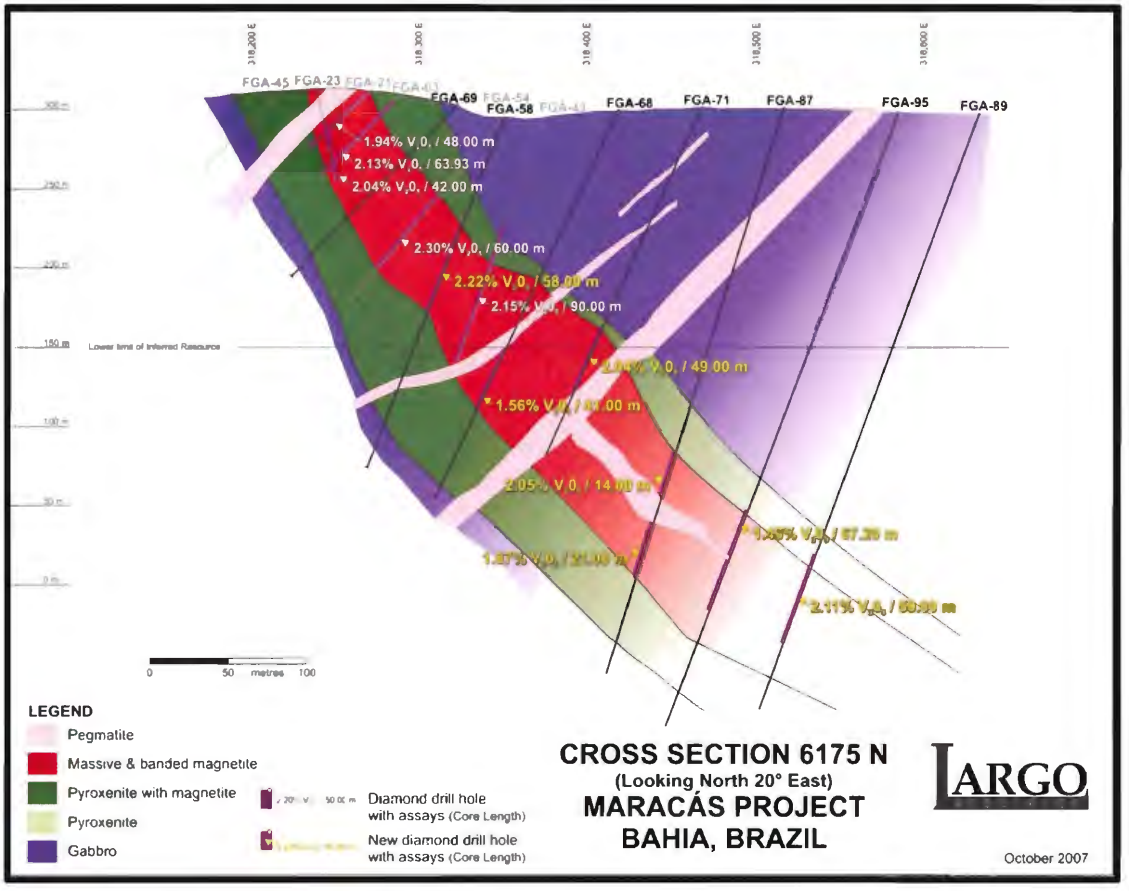

Figure 2.1: Cross section depicting layering within the intrusion, along with late pegmatite (provided by Largo Resources).

The intrusion can be divided into three separate zones; Upper Zone (UZ), Transition Zone (TZ) and Lower Zone (LZ) (Brito et al., n.d.). The lower zone (300-400m thick) consists of medium grained gabbro, some diorite, and minor anorthosite (Sá et al., 2005). Within the gabbro, the clinopyroxene modal proportion increases towards the TZ while plagioclase decreases in grain size approaching the transition zone. Anorthosite is found primarily as a layer near the bottom of the lower zone. The Gulcari A magnetite deposit is found in the lower zone and contains the anomalous PGMs examined in the study (Fig. 2.2, red circle).

The TZ (100-200m thick) is composed of both ultramafic and mafic cumulates. Ultramafic cumulates consist of cumulus olivine, pyroxene, magnetite and ilmenite (Brito et al., n.d.). Rock compositions range from magnetite peridotite, magnetite with pyroxene, and magnetite pyroxenite. Mafic cumulates consist of cumulus plagioclase, pyroxene and minor hypersthene. Microrhythmic sequences of pyroxenite and gabbro are found within the TZ. These sequences show sharp chilled margin contacts. Coarse-grained rocks mark the bottom of the sequence where new magma was injected and cooled quickly creating a fining-upwards sequence. Medium grained gabbroic rocks are found as enclaves that grade into fine-grained blocks. Locally gabbro is found as thin sill-like sheets of diabasic rock (Brito et al., n.d.).

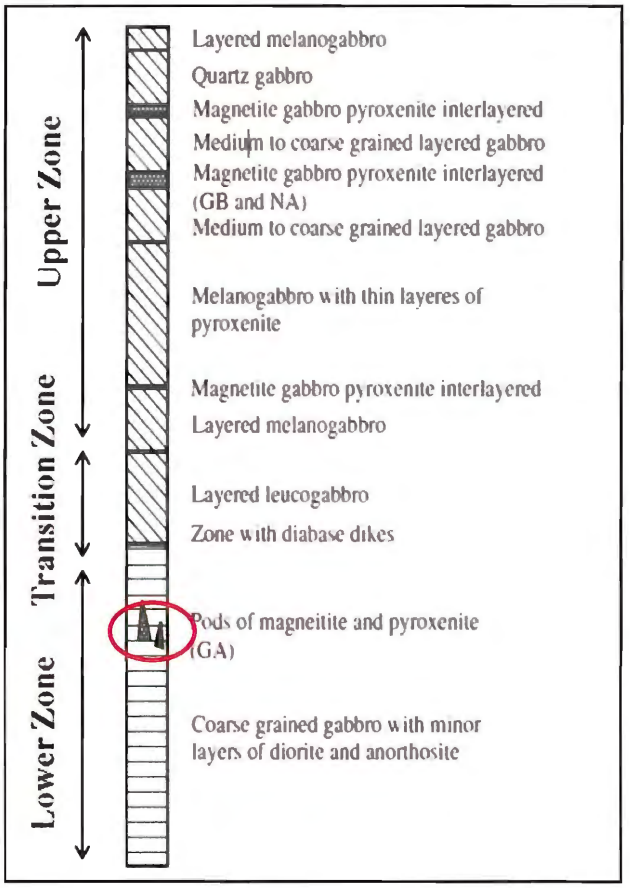

Figure 2.2: Cross section, modified from (Sá et al., 2005) shows the distinction between the upper, transition and lower zone.

The Upper Zone ranges in thickness from 600-1000m. Within the UZ the Gulcari B and Novo Amparo magnetite horizons are found. The upper zone is composed primarily of layered gabbro that ranges from leuco- to melanogabbro. Cyclic units of gabbro, pyroxenite, magnetite-bearing pyroxenite, and magnetite rocks are found in the upper zone (Sá et al., 2005). Pyroxenite layers are thin (centimetres to less than a meter) and usually associated with magnetite bodies.

2.4.1 Metamorphism

Regional metamorphism of the Rio Jacaré intrusion was caused by the Trans-Amazonian Orogeny collisional event (Sá et al., 2005). Around 1.94 Ga, the Gavião and Jequié collided metamorphosing the Rio Jacaré and Contendas-Mirante units. Peak metamorphism is estimated at amphibolite facies, determined by the presence of secondary hornblende (Fig 2.3) and garnet. Replacement of primary magmatic minerals is extensive, with only trace amounts of primary pyroxene and olivine still present. Textural evidence, such as annealing, found in magnetite and ilmenite also suggests that re-crystallization has occurred. Retrograde chlorite, tremolite, actinolite and phlogopite are present. Within the magnetite samples two phases of ilmenite and magnetite are found. A primary sequence of coarse magnetite with exsolution lamellae of ilmenite, is followed by smaller, annealed magnetite, barren of any ilmenite exsolution. Ilmenite, has presumably recrystallized, forming large anhedral intergrowths and inclusions within magnetite.

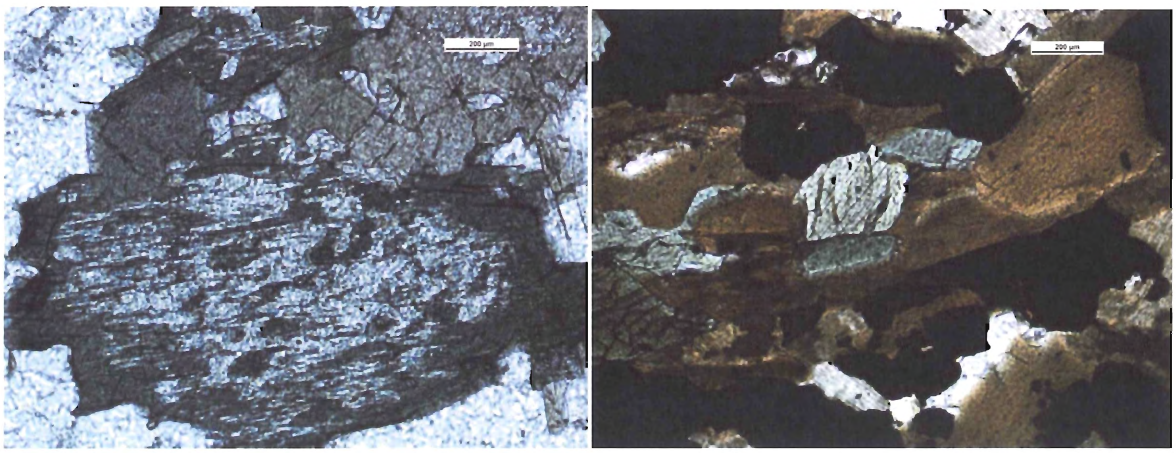

Figure 2.3 Transmitted light photograph A) PPL photograph of hornblende replacing clinopyroxene. B) PPL photograph of metamorphic minerals hornblende and biotite filling in the interstitial space between magnetite and ilmenite.

2.5 Other LMI's associated with Magnetite

2.5.1 Stella Intrusion, South Africa

The 3.05 Ga Stella intrusion is located in the northern part of South Africa. The sill is approximately 12 kilometres long and 1 kilometre thick. Enriched PGE intervals consist of laterally continuous, magnetite hosted reefs (Keays, 2007). Similar to the Rio Jacaré elevated PGE levels occur over a stratigraphic thickness of roughly 100 m. Additionally, the Stella Intrusion also has low copper and sulphur contents in the PGE-enriched zone, increasing sharply, at the upper contact of the PGE-rich zone. There is no clear correlation between concentration of magnetite and concentration of PGE's, although the highest PGE grades do occur in a magnetite rich layer.

The Stella intrusion displays laterally continuous PGE mineralization, while the Rio Jacaré contains magnetite/PGE rich horizons. Pt/Pd values are much lower in the Stella, 0.67 compared to 4.5 in the Rio Jacaré.

2.5.2 Rincón del Tigre Complex, Bolivia

The Rincón del Tigre Complex in Eastern Bolivia is one of the largest mafic-ultramafic intrusions in South America (Prendergast, 2000). The intrusive layered sill is up to 4.6 km thick, and intruded about 990 Ma. PGE's along with other precious metal mineralization are associated with magnetite-gabbro layers found in the upper part of the layered sequence.

Similar to the Rio Jacaré, the sulphide phase boundary is marked by a sharp increase in Fe and V content. All precious metals are located immediately below the sulphide phase boundary. The Pt-subzone is located immediately below the base of the magnetite-gabbro, and 8 m below the Pd-enrichment zone (Prendergast, 2000).

2.6 PGM's in Maracas Deposit

Platinum and palladium mineralization has been confirmed from geochemical assays performed by Largo Resources. Table 1.1 shows enriched values of both Pt and Pd in drill holes on the Maracas project. High grade PGE samples for this study have all been taken from the Gulcari A deposit which is found in the lower zone of the intrusion (Fig. 2.2). Previous work (Brito, n.d.; Sá et al., 2005) provides a textural and mineralogical framework to build upon. Sulphides and arsenides account for up to 1% of rock within magnetite samples (Sá et al., 2005). Sperrylite is the most abundant platinum mineral present, forming subhedral to anhedral crystals. Anomalous platinum values range from 1ppm to 5ppm. The most abundant palladium minerals are Pd-antimonides and Pd-bismuthides. Pt-Pd minerals on average, range in size from 1μm to 10μm.

There are three distinct textural features associated with platinum group mineral formation. The first primary feature is exsolved Pt-Cu alloys within complex sulphide grains. The second feature is exsolution fringes of PGMs that occupy the inner core of arsenide's in intercumulus space. The final feature is PGMs that grow within small fractures inside vanadium rich ilmenite grains (Brito et al., 2005).

Two models have been proposed to describe PGE mineralization within the Rio Jacaré intrusion. The first model proposes orthomagmatic generation of PGMs (Sá et al., 2005), the second focuses on a late stage hydrothermal/metamorphic model for PGE remobilization and recrystallization (Brito et al., n.d.)

Chapter 3: Results

Thirteen polished thin sections reflecting the highest grade Platinum (Pt) and Palladium (Pd) values from drill core at Largo's Gulcari "A" deposit were examined using Dalhousie University's JEOL JXA-8200 Superprobe. Fe-oxides, sulphides, and arsenides were identified using EDS analyses, from which the elemental percentages were calculated and then cross-referenced with a mineral database (www.webmineral.com) to determine the mineral names. Where the obtained composition did not match any of the known minerals from the database, elemental ratios were reported in the formula (i.e., $Ni_{30}Co_{20}S_{50}$). Analyses of smaller grains (<5μm) can potentially introduce peak overlaps, which cause the computer to estimate values for elements that are not present. Considerations were taken to try and reduce analytical error in the reported results. Pt and Pd minerals were identified using EDS, and WDS was used to determine the composition of the grains larger than 10μm. Backscatter Electron (BSE) images were used to examine the textural and spatial relationships between the ore minerals.

For each sample a crystallization sequence was developed based on textural evidence, spatial relationships between grains, and alteration imprints within the sample. The following criteria were used to develop a crystallization sequence.

- Inclusions formed before their corresponding host.
- Large euhedral cumulus minerals formed first in the magma chamber.
- Minerals occupying the interstitial space crystallized after the adjacent cumulus phases.

3.1 Ore Minerals

Ore minerals in the case of this thesis are defined as A) the primary economic mineral of the deposit, or B) a mineral that when present in high enough abundance proves economic. Titaniferous magnetite is vanadium-enriched in the Rio Jacaré intrusion. Vanadium (V) substitutes in the crystal structure of magnetite for iron (Fe). Trivalent vanadium (V^{+3}) has roughly the same ionic size as trivalent iron (Fe^{3+}). Economic grades within the magnetite layer range from 0.46 to 3.0% V_2O_5, with an average grade of 1.27%. These elevated V concentrations (the highest in the world) define magnetite as an ore mineral. Any minerals containing Cu, Ni, Co, Pb, Zn, Ag, Au, Pt, and Pd are considered ore minerals for the purpose of this thesis. Pyrite and ilmenite are gangue minerals often associated with ore minerals. They are grouped in the ore minerals category because the iron-titanium oxide and sulphide minerals, often act as indicators for other more valuable minerals.

**Grain size (e.g. 0.1 to 1.0 mm) refers to the average diameter of the grain measured.*

3.2 Sample Petrography

FGA03-42.27m

Table 3.1 Sample FGA03 42.27 mineralogy.

Mineral	*Chemical Formula*	*Number of Mineral Grains found*	*Average Size (μm)*
Magnetite	Fe_2O_3	Abundant	
Ilmenite	$FeTiO_3$	Abundant	
$Cu_{28}Ni_{31}Co_{14}S_{27}$		1	6
$Ni_{41}Co_{28}S_{31}$		2	2 to 8
Dienerite	Ni_3As	1	5
$Au_{42}As_{58}$		1	20
Sperrylite	$PtAs_2$	2	3-10
Tetraferroplatinum	PtFe	1	3
$Pd_{66}Bi_{34}$		1	2
$Pd_{93}Sb_7$		1	3
$Pd_{54}Ni_{20}Bi_{18}Sb_8$		1	2

Fe-Oxides

Magnetite and ilmenite are the predominant cumulus phases, accounting for 92% of total rock volume in this sample. Ilmenite grains are euhedral and range in size from 0.1 to 1.0 mm. Frequently they form sharp triple point junctions with magnetite grains. Magnetite grains are subhedral and range in size from 0.5 to 2.0 mm.

Sulphides

CuNiCoS and NiCoS are both present in this sample. CuNiCoS occurs as a 6 μm anhedral inclusion within magnetite. Similarly, NiCoS is present as anhedral inclusions within magnetite, ranging in size from 2-8 μm. NiCoS is compositionally similar to the mineral siegenite.

Arsenides

Dienerite and AuAs are present in this sample. Dienerite forms a small anhedral inclusion within magnetite. AuAs also forms a larger 20 μm, anhedral inclusion within magnetite (Fig, 3.1A).

Platinum Group Minerals

Sperrylite and tetraferroplatinum are the platinum phases present, while PdBi, PdSb, and PdNiBiSb are the palladium phases found in this sample. Sperrylite forms an anhedral (3μm) inclusion within ilmenite (Fig, 3.1B), but also forms a larger (10μm) inclusion in magnetite (Fig, 3.1C). Tetraferroplatinum forms a small (3μm) rounded inclusion within magnetite (Fig, 3.1A). PdBi forms a 2μm anhedral inclusion within gangue minerals (Fig, 3.1D). PdSb similarly occurs as a 3μm inclusion sitting in gangue mineralization (Fig, 3.1E). Finally, PdNiBiSb is found as a 2μm anhedral inclusion within an ilmenite grain (Fig, 3.1F).

Crystallization Sequence

I. **Mt-Ilm-Tp-Spy- PdNiBiSb-AuAs-Dt-NiCoS-CuNiCoS**

II. **PdBi-PdSb**

III. **Gangue minerals**

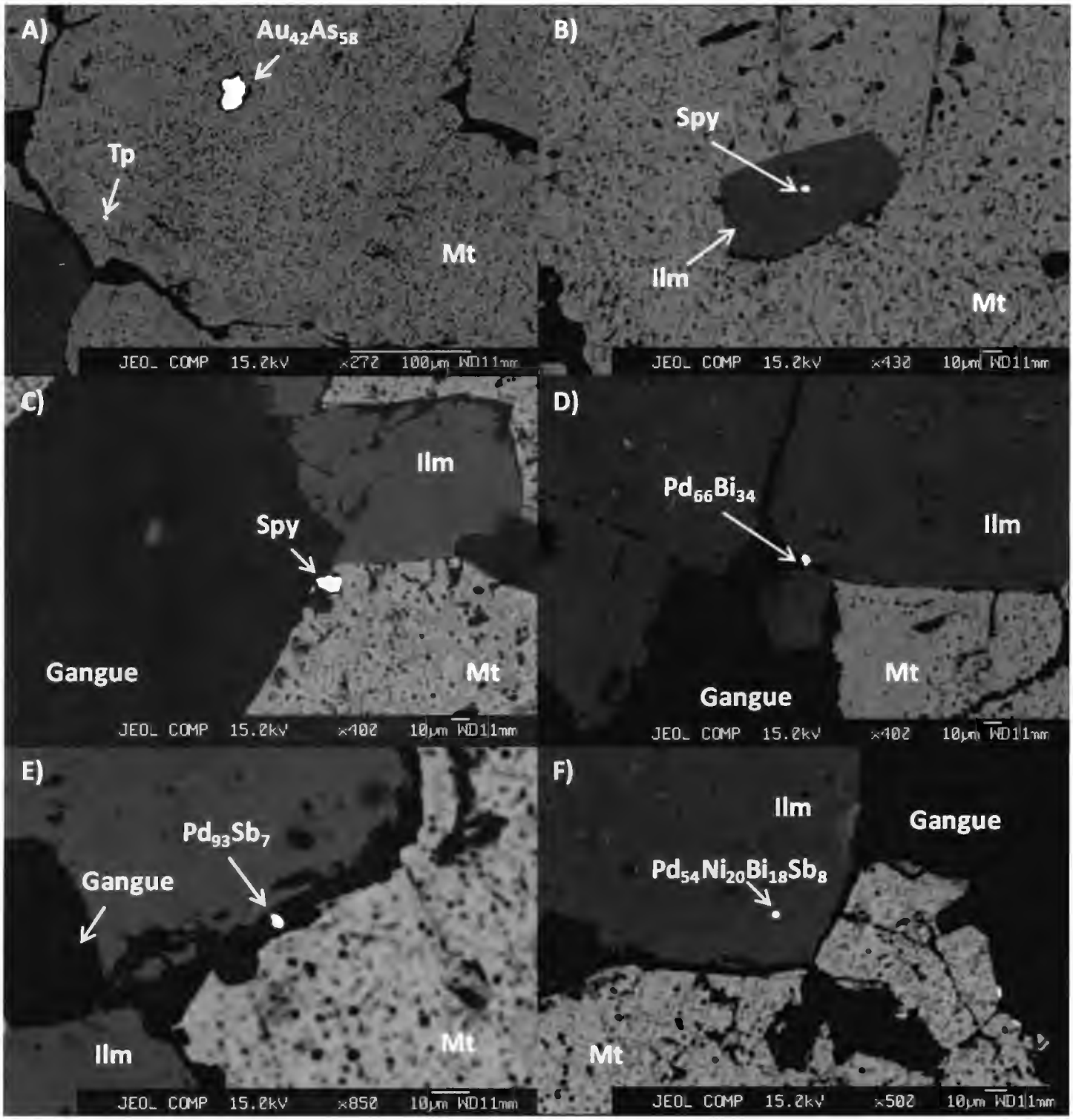

Figure 3.1: BSE images of platinum group elements present within FGA03-42.27m. PGMs are found as inclusions (in Mt/Ilm) or as minute grains located in interstitial space.

FGA04-45.42m

Table 3.2 Sample FGA04 45.42 mineralogy.

Mineral	*Chemical Formula*	*Number of Mineral Grains found*	*Average Size (μm)*
Magnetite	Fe_2O_3	Abundant	
Ilmenite	$FeTiO_3$	Abundant	
$Ni_{30}Co_{22}S_{48}$		+8	30-70
Bravoite	$(Fe,Ni,Co)S_2$	1	50
Orcelite	Ni_5As_3	1	10
$Cu_{55}Zn_{12}Fe_{14}Ni_{19}$		1	10
Tetraferroplatinum	PtFe	1	6
$Pt_{44}As_{10}Fe_{16}Ni_{30}$		1	2

Fe-Oxides

Magnetite and ilmenite are the most abundant ore minerals and form equigranular grains with sharp grain boundary contacts. Grains range in size from 0.2 to 3.0 mm. Magnetite grains specifically show ilmenite exsolution lamellae, on cleavage planes and in intragrain fractures. Some magnetite grains exhibit a "washed" appearance with no exsolution lamellae; corresponding ilmenite grains appear larger and are anhedral.

Sulphides

NiCoS and bravoite are the only sulphides found in this sample. NiCoS is abundant, ranging in size from 30 to 70 μm. Sulphides are located within interstitial space, forming small fractured grains as inclusions, and occasionally as larger grains intergrown with silicates (Fig, 3.2 A&B). NiCoS grains are subhedral and often fractured. Bravoite is present as a host, for a partial inclusion of orcelite. Bravoite is 50 μm in size, subhedral, and located in contact with silicate and ilmenite grains.

Arsenides

Orcelite is the only arsenide present in this slide. Orcelite occurs as a 20 μm anhedral grain. The arsenide is intergrown with gangue minerals, in the interstitial space between cumulus magnetite and ilmenite grains.

Platinum Group Minerals

Platinum-bearing alloys are the only PGE's present in slide FGA 04. The two PGE bearing phases are PtAsNiFe and tetraferroplatinum. Both alloys form anhedral inclusions within large ilmenite grains. The ilmenite host for tetraferroplatinum is fractured (Fig, 3.2D), while the ilmenite host for PtAsNiFe is very clean (Fig, 3.2C). PGE grains are small; ranging in size from 2 to 6 μm. EDS analyses of the PGM alloys was difficult due to the nature of the small grains. The lack of titanium contamination in the analyses suggests that our analyses may still be quite representative of actual platinum grain composition.

Crystallization Sequence

I. **PGE alloys Ilm, Mt**

II. **NiCoS, Br, Or, CuZnFeNi, Gangue minerals**

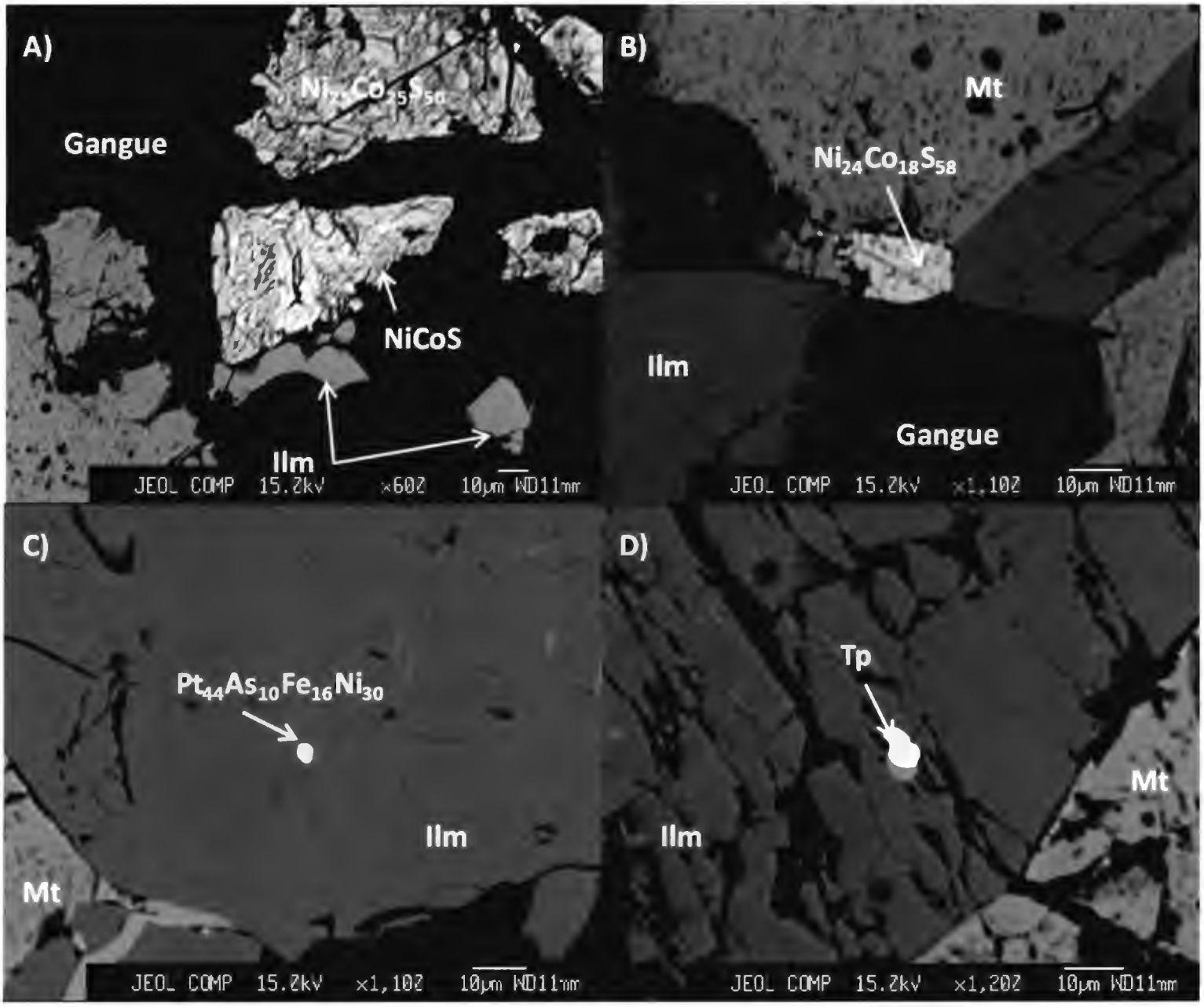

Figure 3.2: BSE images A & B, show irregular sulphides located in interstitial space. C & D show platinum minerals located as inclusions within ilmenite. (FGA04-45.52m)

FGA07-52.18m

Table 3.3 Sample FGA07 52.18 mineralogy.

Mineral	*Chemical Formula*	*Number of Mineral Grains found*	*Average Size (μm)*
Magnetite	Fe_2O_3	Abundant	
Ilmenite	$FeTiO_3$	Abundant	
Chalcopyrite	$CuFeS_2$	3	30-150
Pyrite	FeS_2	1	20
Galena	PbS	2	2-8
Sphalerite	ZnS	1	15
$Ni_{34}Co_{15}S_{51}$		2	15-30
$Ni_{16}Cu_{17}Fe_{21}S_{46}$		1	25
Pentlandite	$(Fe,Ni)_9S_8$	1	20
Orcelite	Ni_5As_2	1	5
$Ni_{35}Co_{10}As_{55}$		1	25
Sperrylite	$PtAs_2$	2	2
Tetraferroplatinum	PtFe	1	2-4

Fe-Oxides

Magnetite and ilmenite are the most abundant ore minerals and form equigranular grains with sharp grain boundary contacts. Grains range in size from 0.2 to 3.0 mm. Ilmenite grains are euhedral and range in size from 0.2 to 0.75 mm. Magnetite grains show ilmenite exsolution lamellae, on cleavage planes, and in intragrain fractures. Magnetite and ilmenite both formed early in the crystallization sequence, as determined by well developed crystal faces and large modal percent of rock volume.

Sulphides

Sulphides present in this sample are located in the interstitial space between early cumulus phases. Sulphides variably consist of clusters of chalcopyrite-sphalerite-NiCoS-NiCuFeS (Fig, 3.3A). Galena however is only found as inclusions or partial inclusions within chalcopyrite. Galena forms anhedral blebs that range in size from 2-8 μm (Fig, 3.3A). Chalcopyrite forms

large 30-150 μm subhedral grains found between magnetite grains (Fig, 3.3A), but also forms between magnetite and secondary silicates (Fig, 3.3C). Pyrite forms a partial inclusion within chalcopyrite, which may indicate an increase in copper during cooling. Sphalerite forms a subhedral grain, 15μm in size, found in contact with magnetite, NiCoS, and NiCuFeS (Fig, 3.3A). NiCoS, likely siegenite, forms subhedral grains, 15-30μm in size. Grains are located at the boundary between magnetite and secondary silicates, or found in clusters with copper sulphides (Fig, 3.3A). NiCuFeS is present as a subhedral grain, 25 μm in size, located between magnetite/ilmenite in interstitial space with secondary silicates. Pentlandite, is found as a 20 μm anhedral grain, located in a sulphide cluster beside chalcopyrite (Fig, 3.3B).

Arsenides

Orcelite and NiCoAs are the two arsenides present in this sample. Ni-arsenides form anhedral grains, located in the interstitial space between cumulus magnetite. The orcelite grain is 5 μm in size, while NiCoAs grain is approximately 25 μm. Small arsenide grains form inclusions in silicates, while larger arsenide grains (NiCoAs) form large crystals intergrown with gangue minerals in interstitial spaces (Fig, 3.3D). Arsenides located in the interstitial spaces are sometimes found associated with sulphides, more often arsenides form individual grains occupying interstitial space.

Platinum Group Minerals

Sperrylite and tetraferroplatinum are the platinum-bearing phases present. Both PGE minerals form inclusions within large magnetite grains. Sperrylite was found as anhedral blebs approximately 4μm in size (Fig 3.3E). Tetraferroplatinum forms an anhedral (5μm) grain (Fig, 3.3F).

Crystallization Sequence

I. **Spy-Tp-Mt-Ilm**

II. **Py and Ga (early inclusions)-Py-Late Cpy(host)-NiCoS-NiCuFeS-Pl-**

III. **Arsenides-Gangue minerals**

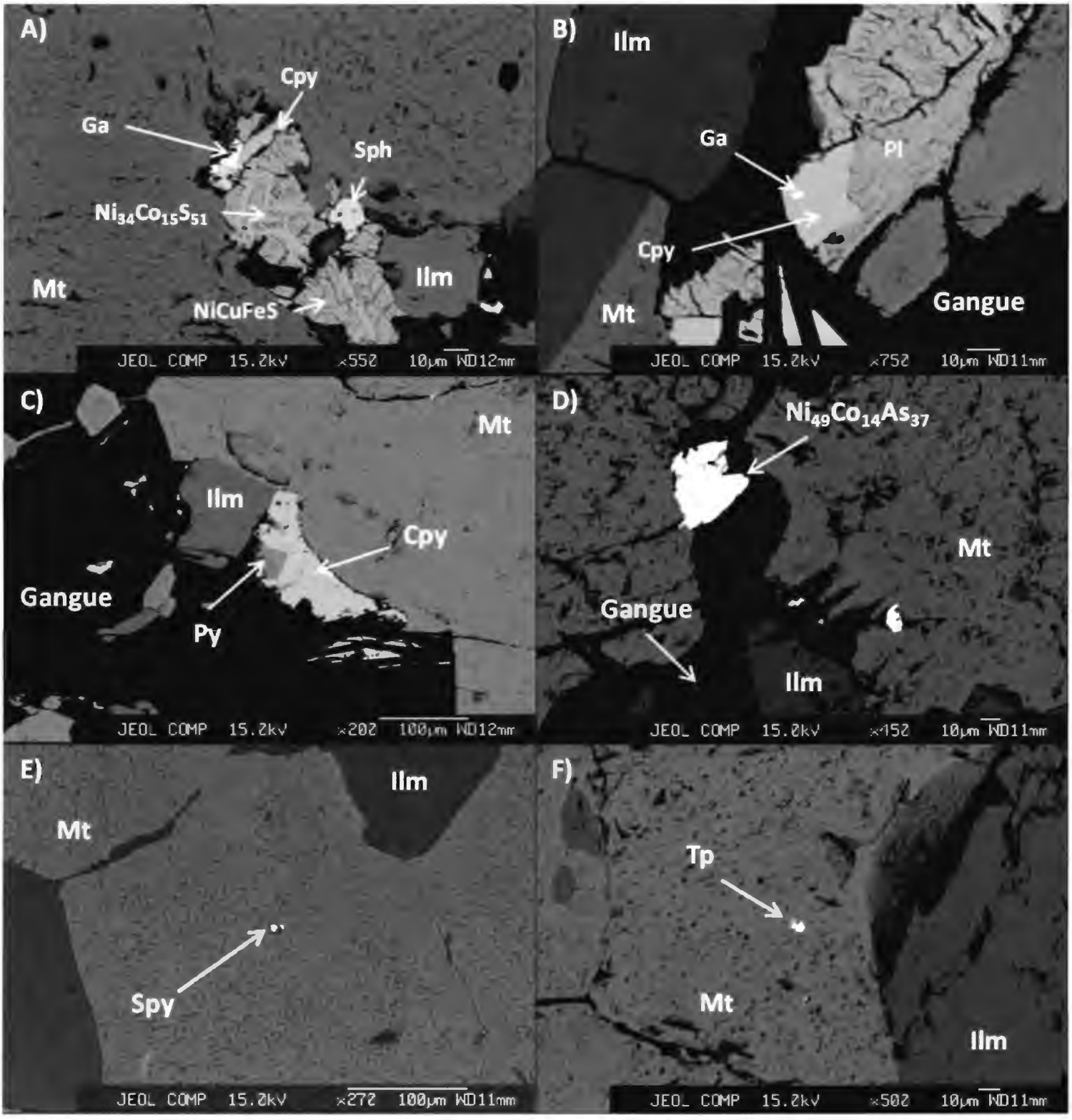

Figure 3.3: Early Spy and Tp seen in E & F. Late sulphide clusters found in interstitial space, A, B & C. (FGA07 -52.18m)

FGA14-22.90m

Table 3.4 Sample FGA14 22.90 mineralogy.

Mineral	*Chemical Formula*	*Number of Mineral Grains found*	*Average Size (μm)*
Magnetite	Fe_2O_3	Abundant	
Ilmenite	$FeTiO_3$	Abundant	
Chalcopyrite		1	2
Co-rich Pentlandite	$(Fe,Ni)_9S_8$	5	3
CuFe		1	10
Native Copper	Cu	1	10

In this slide, no arsenides, bismuthides, antimonides, or PGMs were found. The geochemical assay for this slide reports elevated levels of Pt (1803 ppb) and lower levels of Pd (103 ppb).

Fe-Oxides

Magnetite and ilmenite are the most abundant ore minerals in the sample, accounting for more than 90% of the minerals present. Ilmenite grains in the sample are subhedral to anhedral and smaller in size (0.1 to 0.5 mm). Ilmenite grains often appear fractured and filled in by silicate minerals. Grain boundary contacts between the Fe-oxides are irregular, with silicate mineralization filling the void space. Magnetite grains, generally subhedral, are on average 1.0 mm in size. In specific zones, magnetite displays exsolution lamellae of ilmenite.

Sulphides

Cobalt-rich pentlandite and chalcopyrite are present. Cobalt-rich pentlandite is the most abundant phase forming small (3μm) anhedral inclusions within an ilmenite. A chalcopyrite grain (2μm) also forms an anhedral inclusion within a larger ilmenite host.

Copper & Copper Alloys

Native copper is present in the slide as anhedral grains within interstitial silicate space (Fig, 3.4A). Grains range in size from 1-15 μm. CuFe alloys were found along the grain boundary of connecting magnetite grains (Fig, 3.4B). Grains were subhedral and 15 μm in size.

Crystallization Sequence

I. **Mt-Ilm-Cpy-CuFe-Pl**

II. **Gangue minerals & Native Copper**

FGA43-104.68m

Table 3.5 Sample FGA43 104.68 mineralogy.

Mineral	*Chemical Formula*	*Number of Mineral Grains found*	*Average Size (μm)*
Magnetite	Fe_2O_3	Abundant	
Ilmenite	$FeTiO_3$	Abundant	
Chalcocite	Cu_2S	3	15
Co-rich Pentlandite	$(Fe,Ni)_9S_8$	8	15
$Ni_{39}Co_5As_{56}$		5	20
NiSb		1	8

During analyses of the slide no PGMs were found, although geochemical assay produced results of 4300ppb combined Pt & Pd.

Fe-Oxides

Magnetite and ilmenite form abundant cumulus grains with sharp grain boundary contacts. Ilmenite occurs as subhedral to anhedral grains ranging in size from 0.1 to 0.4 mm. Locally,

anhedral ilmenite fills in the interstitial space between cumulus magnetite-ilmenite grains. Magnetite occurs as coarse grained (>1.0 mm) euhedral crystals.

Sulphides

Chalcocite and cobalt-rich pentlandite were present in this slide, often associated as mineral clusters within interstitial space (Fig, 3.5A). Chalcocite forms anhedral 15 μm crystal aggregates. Cobalt-rich pentlandite forms similar 15 μm anhedral aggregates found in close proximity to chalcocite grains.

Arsenides

NiCoAs is present in abundance, located on the magnetite-ilmenite boundary between gangue mineralization (Fig, 3.5B). The arsenide forms roughly 20 μm anhedral grains.

Ni-Alloy

NiSb, likely breithaupite, is present as a single anhedral bleb partially enclosed by NiCoAs (Fig, 3.5B).

Crystallization Sequence

I. Mt-Ilm

II. NiSb(early)-NiCoAs(later)-Ch-Pl

III. Gangue minerals

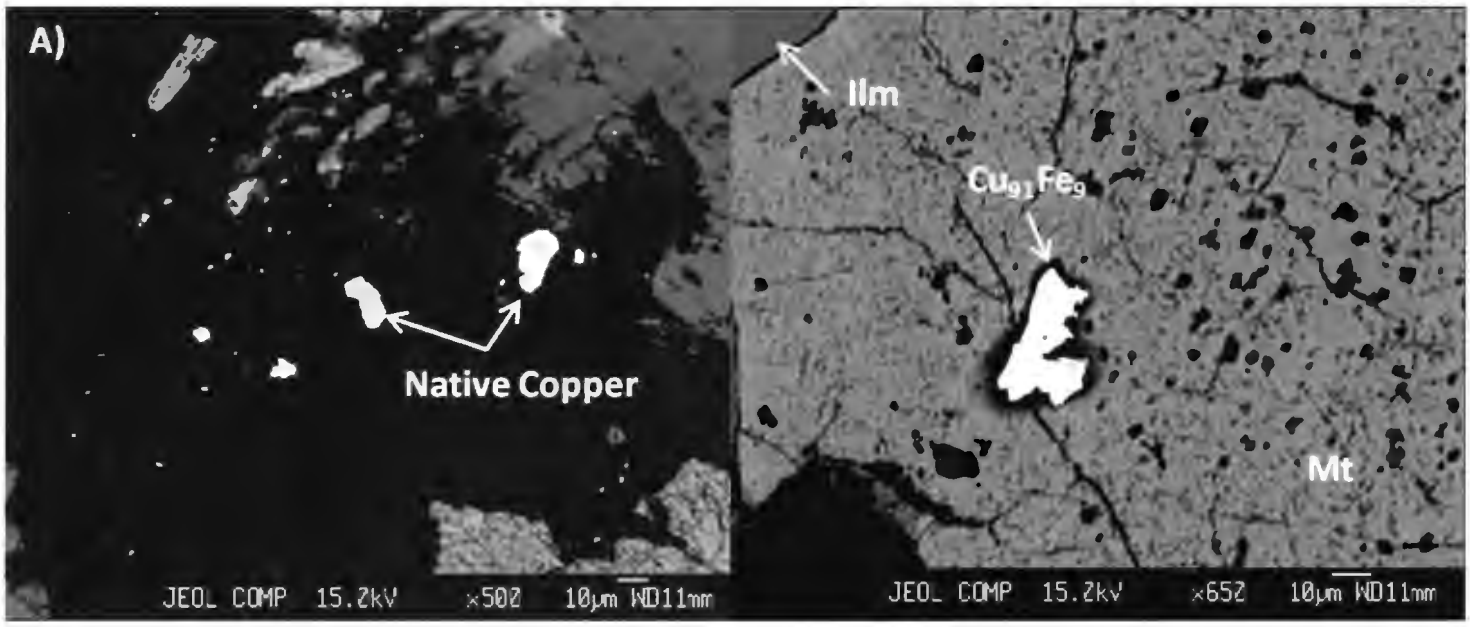

Figure 3.4: Late copper, found intergrown with silicate minerals (A). Early copper alloy found as inclusion within magnetite, and associated silicate halo (B). (FGA14-22.90m)

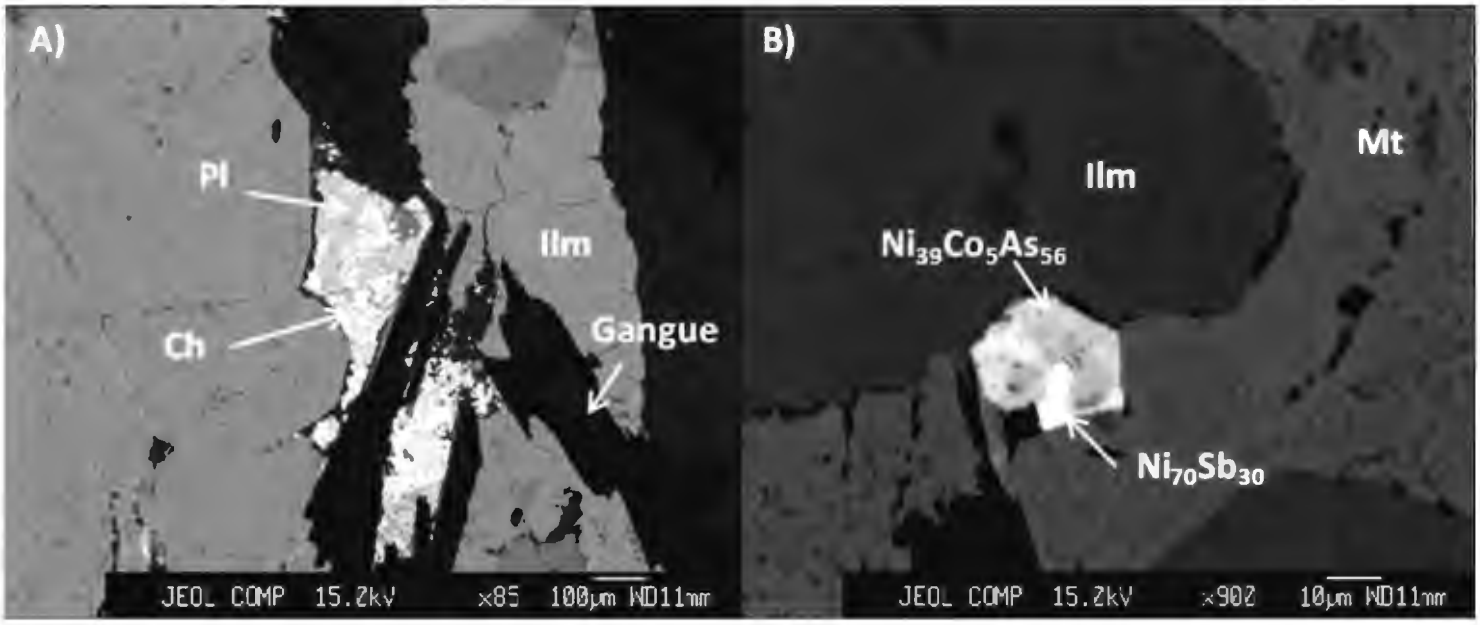

Figure 3.5: Sulphide cluster composed of pentlandite and chalcocite (A). Nickel arsenide with NiSb inclusion, located at the grain boundary contact between magnetite and ilmenite. (FGA43-104.68m)

FGA17-82.14m

Table 3.6 Sample FGA17 82.14 mineralogy.

Mineral	*Chemical Formula*	*Number of Mineral Grains found*	*Average Size (μm)*
Magnetite	Fe_2O_3	Abundant	
Ilmenite	$FeTiO_3$	Abundant	
$Ni_{23}Co_{29}S_{48}$		+5	10
Co-rich Pentlandite	$(Fe,Ni)_9S_8$	1	30
Orcelite	Ni_5As_3	+5	15
$Ni_{37}Co_8As_{55}$		+5	25
$Ni_{91}Fe_7P_2$		1	10
$Ni_{46}Sb_{54}$		1	10
$Cu_{76}Fe_{24}$		1	10
$Pt_{17}Sb_{14}Sn_{21}Ni_{18}Co_9S_{21}$		1	2

Fe-Oxides

Ilmenite grains are subhedral and on average 0.3 mm in diameter. Grains found as inclusions within silicates are rounded, whereas cumulus ilmenite shows sharp grain boundary contacts. Magnetite grains display ilmenite exsolution lamellae, with a 60/120° degree orientation. Magnetite is often subhedral, with an average size of 1.0 mm. Some magnetite grains exhibit a "washed" appearance with no exsolution lamellae, and associated larger anhedral ilmenite grains.

Sulphides

NiCoS and cobalt-rich pentlandite are the sulphides phases present. NiCoS is found abundantly as inclusions within silicates. Sulphides form anhedral grains approximately 40 μm in size. Cobalt-rich pentlandite is also present as an inclusion within silicates. The grain analysed was subhedral and approximately 30 μm in size.

Arsenides

NiCoAs and orcelite are abundant. NiCoAs forms anhedral grains on the boundary between washed magnetite's and secondary silicates (Fig, 3.6A,B). NiCoAs grains are roughly 20 μm in diameter. NiCoAs, possibly nickelskutterudite, although compositionally it contains less arsenic and more nickel. Orcelite forms elongate (4-8μm) grains along the boundaries between ilmenite and magnetite grains. Additionally orcelite is present as larger (60μm) grains, located as inclusions within magnetite.

Ni-alloys and Ni-phosphates

NiSb, and NiFeP are the minerals present. NiSb is associated with NiCoAs and is found in the interstitial space between magnetite and silicates (Fig, 3.6B). NiSb forms an anhedral bleb 10 μm in size. NiSb is possibly the mineral breithauptite, but compositionally contains more nickel and less antimony. NiFeP is found as a single anhedral inclusion inside a magnetite grain. The phosphate resides inside a magnetite grain, between two elongate ilmenite lamellae (Fig, 3.6D).

Cu-alloys

CuFe forms as an anhedral inclusion within a washed magnetite grain (Fig, 3.6C).

Platinum Group Minerals

PtSbSnNiCoS is the only PGM present in this slide. The Pt-alloy is found as an inclusion inside a NiCoS grain. The grain is 2 μm in size and forms an anhedral bleb.

Crystallization Sequence

I. **CuFe-NiFeP-Mt-Ilm-Pt-alloy-Or(inclusion)**
II. **NiSb-NiCoS-Pl-NiCoAs-Or interstitial space)**
III. **Gangue minerals**

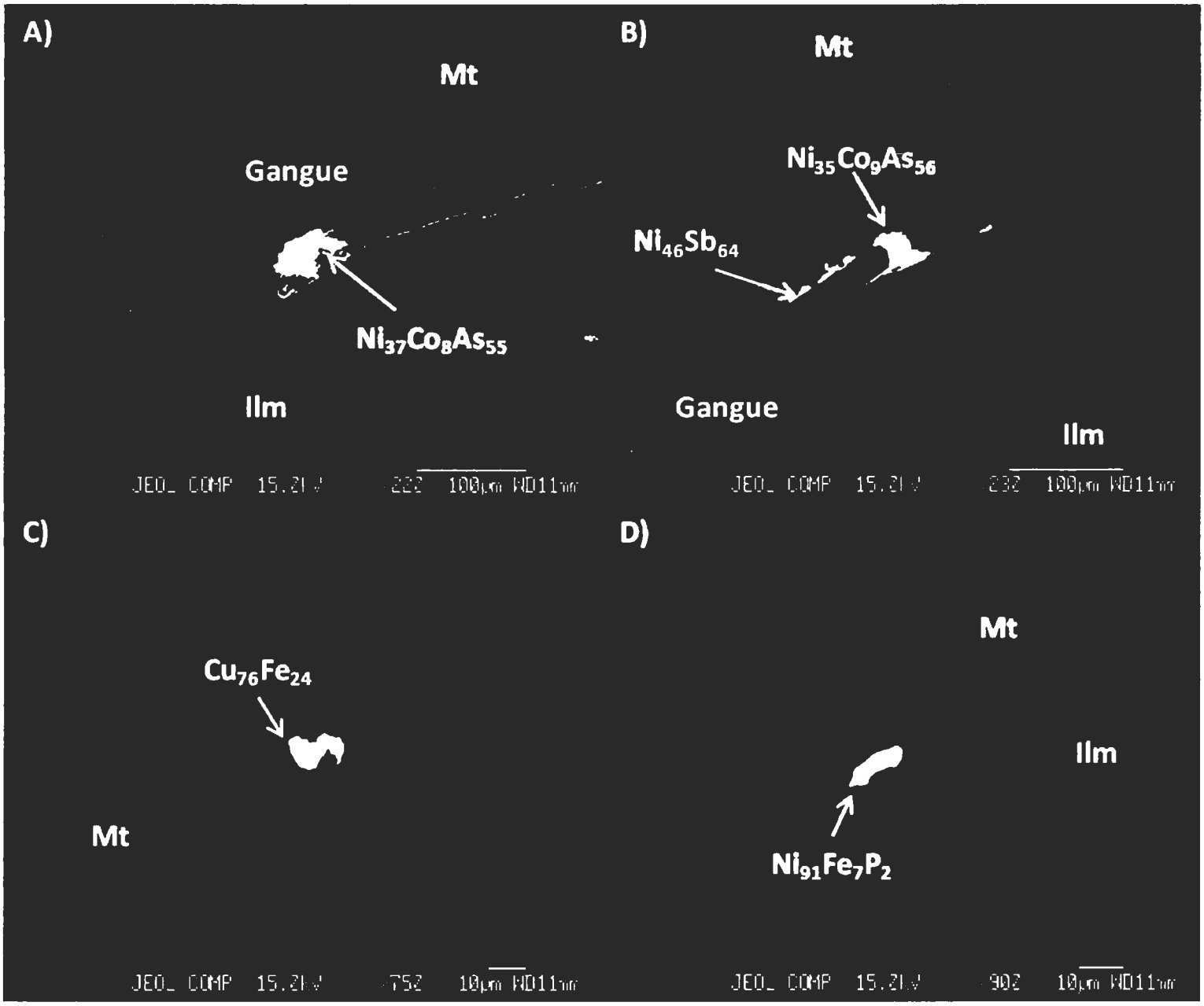

Figure 3.6: Early copper alloys and phosphates present as inclusions (C & D). Late arsenides and antimonides seen in A & B. (FGA17-82.24m)

FGA20-52.72m

Table 3.7 Sample FGA20 52.72 mineralogy.

Mineral	*Chemical Formula*	*Number of Mineral Grains found*	*Average Size (μm)*
Magnetite	Fe_2O_3	Abundant	
Ilmenite	$FeTiO_3$	Abundant	
Sphalerite	ZnS	1	3
$Ni_{39}Co_{32}S_{29}$		6	2-60
Co-rich Pentlandite	$(Fe,Ni)_9S_8$	1	6
$Ni_{64}Co_9As_{27}$		1	2
Dienerite	Ni_3As	1	5
Krutovite	$NiAs_2$	1	5
Sperrylite	$PtAs_2$	2	2-5
$Pt_{59}Fe_{18}Ni_{23}$		1	5

Fe-Oxides

Magnetite and ilmenite are abundant cumulus minerals present in the sample. Combined, they account for 86% of the total rock volume. Ilmenite forms sub-rounded to rounded grains with an average size of 0.3 mm. Magnetite grains are subhedral and on average 0.75 mm.

Sulphides

Sphalerite, NiCoS, and cobalt-rich pentlandite are found in this sample. Sphalerite forms a small (3μm) anhedral inclusion within magnetite (Fig, 3.7A). NiCoS grains are abundant, and form in two different settings. Small, 2 μm anhedral grains form as inclusions within magnetite (Fig, 3.7B), while larger (60μm) grains form subhedral grains intergrown with silicate minerals in interstitial space. Cobalt-rich pentlandite also forms a small (6μm) anhedral inclusion within magnetite.

Arsenides

NiCoAs, krutovite and dienerite are the arsenide phases present in this slide. NiCoAs is located as a small (2μm) anhedral inclusion within magnetite. Krutovite and dienerite are also found as small, 5 μm anhedral inclusions within magnetite (Fig, 3.7C).

Platinum Group Minerals

Sperrylite and PtFeNi are the PGM phases present in this slide. Both sperrylite and PtFeNi are found as small (2-5μm) anhedral inclusions within ilmenite (Fig, 3.7D,E,F).

Crystallization Sequence

I. **Mt-Ilm-Spy-PtFeNi-NiCoS(inclusions)-Pl-Sph-NiCoAs-Kt-Dt**

II. **NiCoS(large grains)-Gangue minerals**

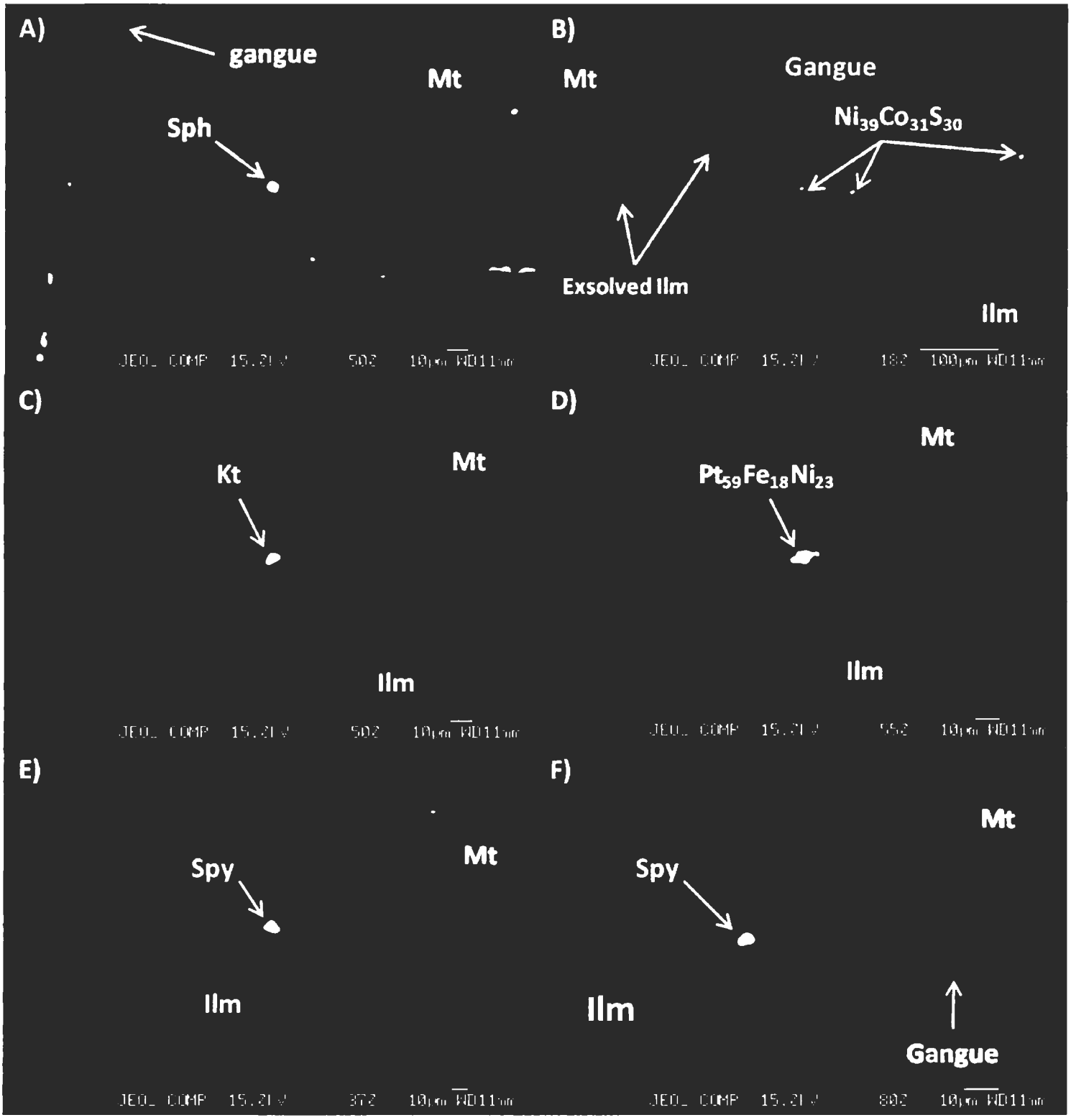

Figure 3.7: Early ore minerals present as inclusions within magnetite and ilmenite. The presence of sulphide and arsenide as inclusions in Mt and Ilm is unusual when compared to the other thin sections (A, B, C). (FGA20-52.72m)

FGA20-53.88m

Table 3.8 Sample FGA20 53.88 mineralogy.

Mineral	*Chemical Formula*	*Number of Mineral Grains found*	*Average Size (μm)*
Magnetite	Fe_2O_3	Abundant	
Ilmenite	$FeTiO_3$	Abundant	
$Ni_{39}Co_{36}S_{25}$		2	2
$Ni_{69}S_{31}$		1	20
Pentlandite	$(Fe,Ni)_9S_8$	1	4
Orcelite		5	5
$Au_{48}As_{52}$		1	10
Sperrylite	$PtAs_2$	2	10
Tetraferroplatinum	PtFe	1	5
$Pt_{44}Pd_{18}Sn_{18}Cu_{10}S_{10}$		1	3

Fe-Oxides

Magnetite and ilmenite are present as abundant (+90% modal rock volume) cumulus subhedral to euhedral grains. Ilmenite is present as both cumulus grains, and as exsolution lamellae (60/120° orientation) within coarse grained magnetite crystals. As individual grains, ilmenite ranges in size from 0.1 to 0.5 mm. Secondary ilmenite grains form anhedral grains, ~30-50 μm is size, found associated with "washed" magnetite grains. Magnetite ranges in size from 0.3 to 1.0 mm.

Sulphides

NiCoS, NiS and cobalt-rich pentlandite are present in this sample. NiCoS forms small, 2 μm anhedral inclusions within magnetite. A second phase of NiCoS is found as a thin anhedral mineral filling the interstitial space between magnetite grains (Fig, 3.8C). NiCoS is likely siegenite, although the chemical composition contains more cobalt and less sulphur. NiS is likely the mineral millerite. It forms a subhedral, 20 μm grain located in the interstitial space

between magnetite crystals intergrown with gangue minerals (Fig, 3.8D). Pentlandite forms a small 4μm inclusion within magnetite.

Arsenides

AuAs and orcelite are both present in this sample. AuAs is found as a 10 μm anhedral inclusion within a secondary ilmenite grain (Fig, 3.8A). Orcelite forms a small (5μm) inclusion within magnetite.

Platinum Group Minerals

Sperrylite, tetraferroplatinum and PtPdSnCuS are the PGMs present in this sample. Sperrylite is found as 10 μm anhedral grains located at the boundary between ilmenite, magnetite and gangue minerals (Fig, 3.8E). Sperrylite forms as inclusions and partial inclusions within secondary ilmenite (discussed above). Tetraferroplatinum forms 5 μm inclusions within a primary magnetite grain (Fig, 3.8F). PtPdSnCuS is present as an inclusion within magnetite, close to the grain boundary with ilmenite (Fig, 3.8B). The grain is approximately 3 μm, and anhedral.

Crystallization Sequence

I. **Mt-Ilm (primary)-Tp-PtPdSnCuS-Or-Pl**

II. **Ilm (secondary)-Spy-NiCoS-NiS-AuAs**

III. **Gangue minerals**

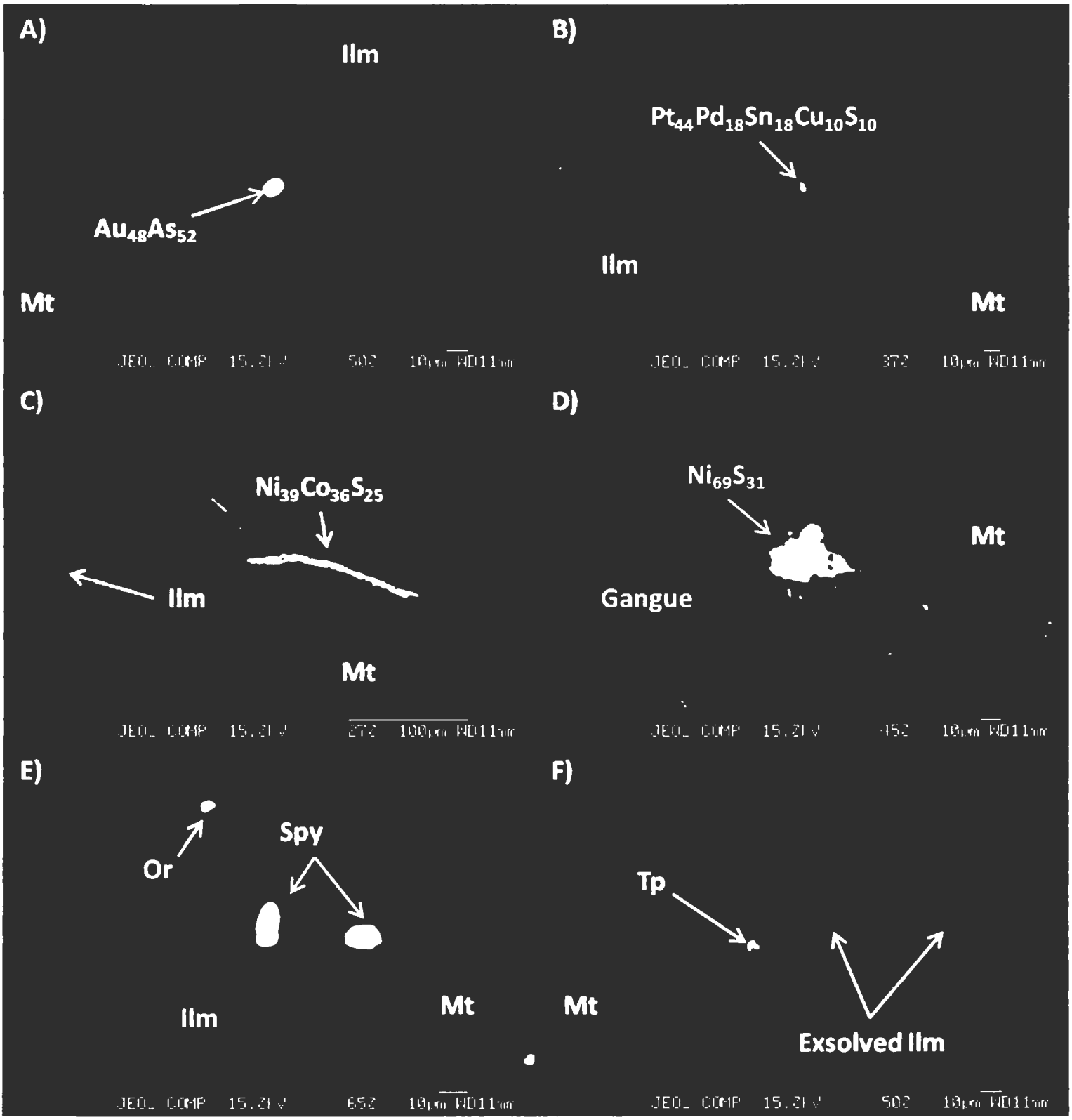

Figure 3.8: Early platinum mineralization present in F), while late sulphides fill in grain-boundary contacts C). (FGA20 -53.88m)

FGA23-49.80m

Table 3.9 Sample FGA23 49.80 mineralogy.

Mineral	*Chemical Formula*	*Number of Mineral Grains found*	*Average Size (μm)*
Magnetite	Fe_2O_3	Abundant	
Ilmenite	$FeTiO_3$	Abundant	
Pyrite	FeS_2	1	15
Sphalerite	ZnS	2	20
Galena	PbS	1	1
Dienerite	Ni_3As	1	3
$Ni_{92}Fe_8$		1	10
$Pt_{33}As_5Fe_{38}Ni_{24}$		1	3

Fe-Oxides

Magnetite and ilmenite are the most abundant (90% modal rock volume) ore minerals and form cumulus phases with sharp grain boundary contacts. Often grain boundary contacts form sharp triple point junctions with 120° orientations. Magnetite grains often show ilmenite exsolution lamellae. Magnetite grains are coarse, euhedral, and on average >1.0 mm. Ilmenite is found as smaller (0.1 to 0.5 mm), subhedral to anhedral grains.

Sulphides

Pyrite, sphalerite and galena are present in this slide. Pyrite forms an anhedral, 15 μm inclusion inside ilmenite (Fig, 3.9A). Sphalerite, however, is located at grain-boundary contacts between magnetite and ilmenite (Fig, 3.9A). Galena is present as a tiny (1μm) anhedral inclusion within magnetite. Generally sulphides form clusters, located within the interstitial space between cumulus minerals.

Arsenides

Dienerite is the only arsenide present in the slide. Dienerite forms subhedral grains approximately 3 μm in size, located at the boundary between magnetite and ilmenite exsolution lamellae (Fig, 3.9B).

Ni-Alloy

NiFe is found as small (10μm) subhedral grain present in interstitial space. The grain forms as an intergrowth associated with gangue minerals (Fig, 3.9C).

Platinum Group Minerals

PtAsNiFe is the only platinum phase found. PtAsNiFe forms a rounded bleb roughly 3 μm in diameter. The platinum phase is present as an inclusion within magnetite, 6 μm from the magnetite-magnetite grain boundary (Fig, 3.9D).

Crystallization Sequence

I. **Mt-Ilm-PtAsNiFe-Py-Ga**

II. **Sph-Dt**

III. **Gangue minerals**

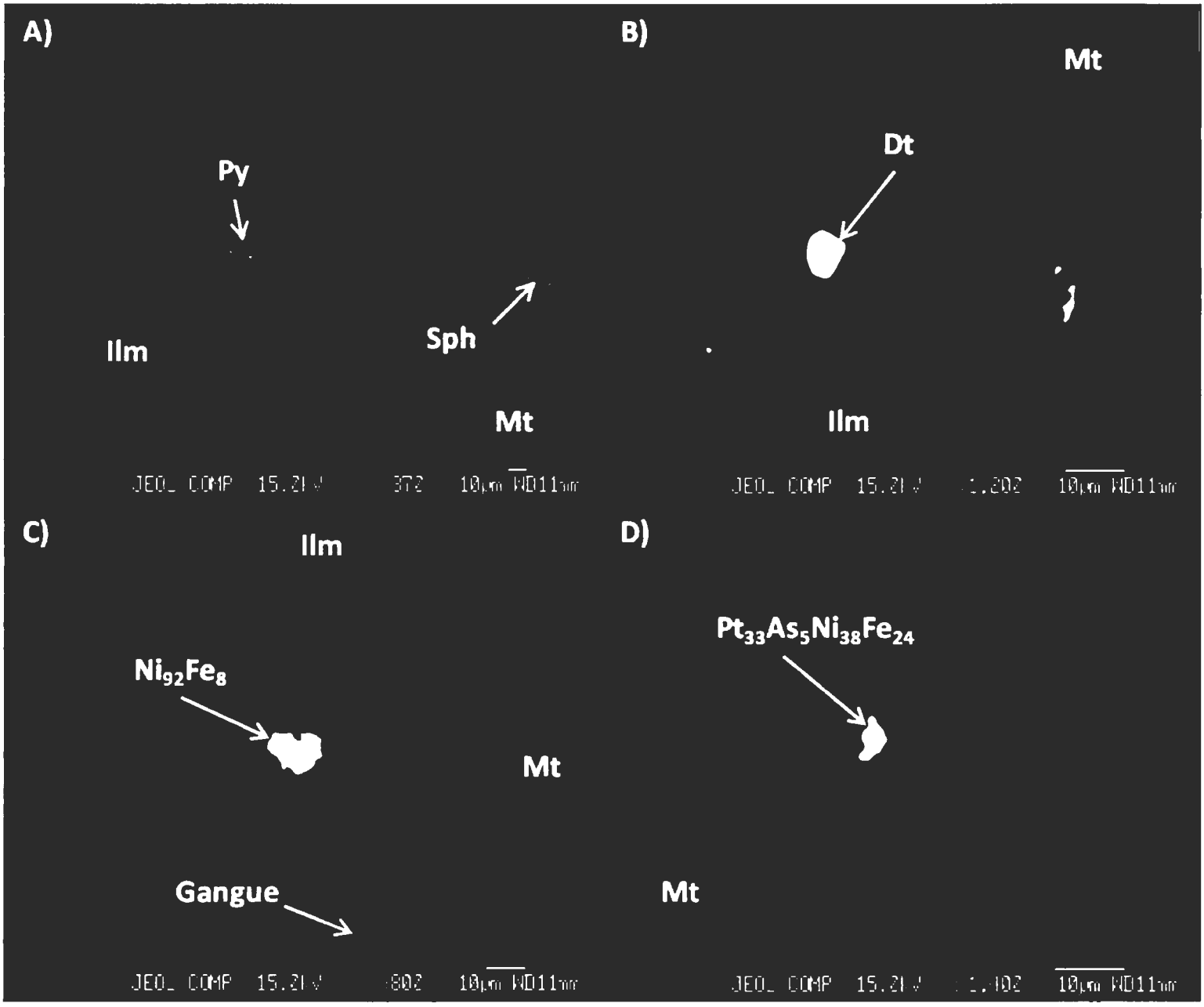

Figure 3.9: BSE images above show the location, shape and association of ore minerals found in slide FGA23-49.80m

FGA80-22.52m

Table 3.10 Sample FGA80 22.52 mineralogy.

Mineral	*Chemical Formula*	*Number of Mineral Grains found*	*Average Size (μm)*
Magnetite	Fe_2O_3	Abundant	
Ilmenite	$FeTiO_3$	Abundant	
Chalcopyrite	$CuFeS_2$	5	50-100
Sphalerite	ZnS	2	20-40
Chalcocite	Cu_2S	3	20
$Ni_{24}Co_{22}S_{54}$		1	20
Cobaltite	CoAsS	1	20
Alloclasite	(Co,Fe)AsS	1	25
Sperrylite	$PtAs_2$	6	1-10
$Pd_{31}Te_{42}Bi_{27}$		2	8
$Pd_{57}Bi_{32}Sb_{11}$		1	10
AuAg		1	10

Fe-Oxides

Magnetite and ilmenite are the most abundant ore minerals in this sample. Magnetite and ilmenite show distinct alteration where close to secondary silicates. Grains are highly fractured, and voids are filled with gangue. Both magnetite and ilmenite form sub- to anhedral grains and are smaller in size when compared to other samples. Ilmenite grains range from 0.05 to 0.3 mm. Magnetite grains range in size from 0.3 to 0.5 mm.

Sulphides

Chalcopyrite, sphalerite, chalcocite, NiCoS and alloclasite are present in this sample. Chalcopyrite forms large (50-100μm), subhedral grains in interstitial space, intergrown with gangue minerals. Chalcopyrite also present in the core of zoned grains containing chalcocite rims (Fig, 3.10A). Chalcocite is found in interstitial space, near the boundary of magnetite and ilmenite grains forming 20 μm subhedral crystals. Sphalerite forms partial inclusions within chalcopyrite, as 20-40 μm subhedral grains. Partial inclusions of sphalerite indicate earlier

formation compared to chalcopyrite. Furthermore sphalerite is present in interstitial space surrounded by gangue minerals. NiCoS is found as a 20 μm anhedral grain located in interstitial space intergrown with gangue minerals. Cobaltite forms a euhedral 20 μm grain present in interstitial space, intergrown with gangue minerals (Fig, 3.10B). Alloclasite forms a subhedral, 25 μm grain located on the boundary between ilmenite and gangue mineralization (Fig, 3.10D).

Arsenides

No arsenide's were found in this slide other than those associated with PGMs. PGMs forming arsenides are described separately below.

Platinum Group Minerals

Both platinum and palladium minerals are present in this slide. Platinum minerals are associated with arsenic while palladium minerals are associated with bismuth/tellurium and antimony. Sperrylite grains range in size from 1 to 150 μm. The majority of sperrylite grains are 1-10 μm (Fig, 3.10B,D). Sperrylite is found primarily as inclusions within gangue minerals. Minor amounts of sperrylite are present as inclusions within alloclasite (Fig, 3.10D). PdBiTe grains are subhedral and 8μm in size and located in interstitial space at the boundary between magnetite, ilmenite and gangue minerals (Fig, 3.10F). PdBiSb grains, also anhedral, form inclusions within large gangue minerals (Fig, 3.10E). The PdBiSb mineral appears to have exsolved (precipitated) along the cleavage plane of the gangue mineral.

Crystallization sequence

I. **Mt-Ilm**
II. **Spy-Cb-PdBiSb-PdTeBi-NiCoS-Sph(inclusion)Cpy-Ch(outer rim)**
III. **Gangue minerals-Al**

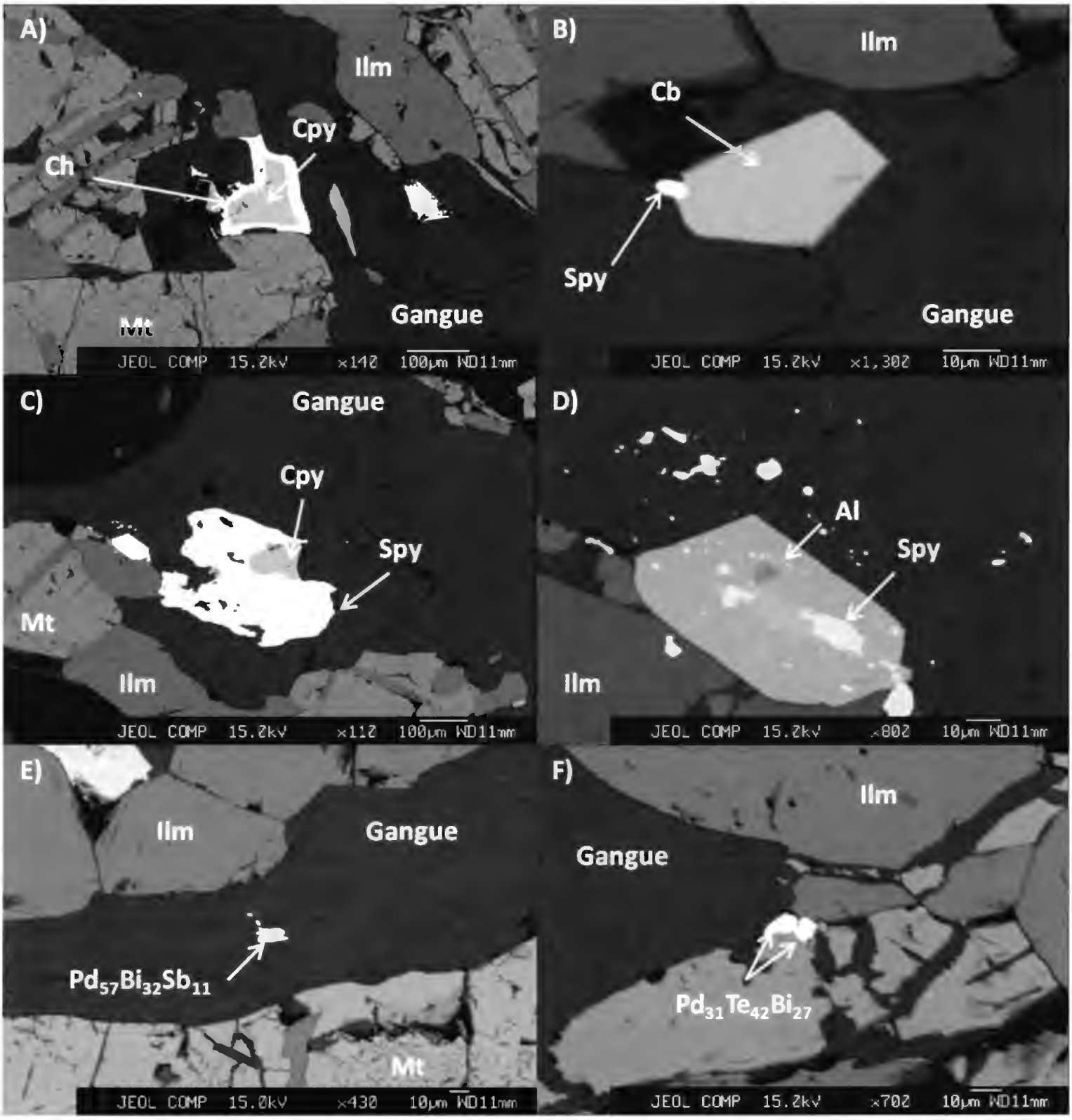

Figure 3.10: BSE images above show the location, shape and association of ore minerals found in FGA80-22.52m

FGA58-140.40m

Table 3.11 Sample FGA58 140.40 mineralogy.

Mineral	*Chemical Formula*	*Number of Mineral Grains found*	*Average Size (μm)*
Magnetite	Fe_2O_3	Abundant	
Ilmenite	$FeTiO_3$	Abundant	
Sphalerite	ZnS	2	20
$Ni_{23}Co_{28}S_{49}$		2	30
Co-rich Pentlandite	$(Fe,Ni)_9S_8$	5	15
$Ni_{48}Co_{14}As_{38}$		1	25
Orcelite	Ni_5As_2	5	10-30
AuAg		1	6
Sperrylite	$PtAs_2$	2	2-5
Niggliite	PtSn	2	5-8
Paolovite	Pd_2Sn	2	6

Fe-Oxides

Magnetite and ilmenite form cumulus phases, accounting for 90% of minerals present. Magnetite grains show ilmenite exsolution lamellae, on cleavage planes, forming 60°/120° orientations. Some magnetite grains exhibit a "washed" appearance with no exsolution lamellae and larger resorbed ilmenite grains. Ilmenite grains are anhedral and range in size from 0.1 to 0.4 mm. Magnetite grains on average are 1.0 mm.

Sulphides

Sphalerite, NiCoS and cobalt-rich pentlandite are found in this sample. Sphalerite forms a 20 μm subhedral inclusion within magnetite, sitting in close proximity to ilmenite exsolution lamellae. NiCoS is as a 30 μm anhedral grain at the boundary between ilmenite and gangue mineralization (Fig, 3.11A). Cobalt-rich pentlandite is abundant, forming small (15μm) subhedral inclusions within magnetite.

Arsenides

Orcelite is the dominant arsenide phase present in the slide. Orcelite forms sub- to anhedral grains that range in size from 10 to 30 μm. Grains are located in the interstitial space between magnetite grains (Fig 3.11B), and along grain boundaries between ilmenite and gangue mineralization (Fig, 3.11E). NiCoAs is present as a 25 μm anhedral inclusion within gangue mineralization (Fig, 3.11D). NiCoAs is also a host for a niggliite inclusion.

Platinum Group Minerals

Sperrylite forms small (2-5μm) anhedral inclusions within gangue minerals (Fig, 3.11D), and in interstitial space between magnetite and ilmenite, at grain boundaries (Fig, 3.11C). Pt-Sn mineralization is found in the form of niggliite. Niggliite forms small (10μm), anhedral grains associated with Ni-arsenides as partial inclusions (Fig, 3.11D,E). Tin saturation appears abundant in this part of the intrusion with Pd-Sn minerals forming as well. This is the only slide with Tin minerals present. Paolovite grains are similar in size and shape to sperrylite, and occur in gangue minerals at the boundary between ilmenite and gangue mineralization (Fig, 3.11F).

Crystallization Sequence

I. **Mt-Ilm-Sph-Pl-AuAg**

II. **NiCoS-Nt**

III. **NiCoAs-Spy-Pv-Or**

IV. **Gangue minerals**

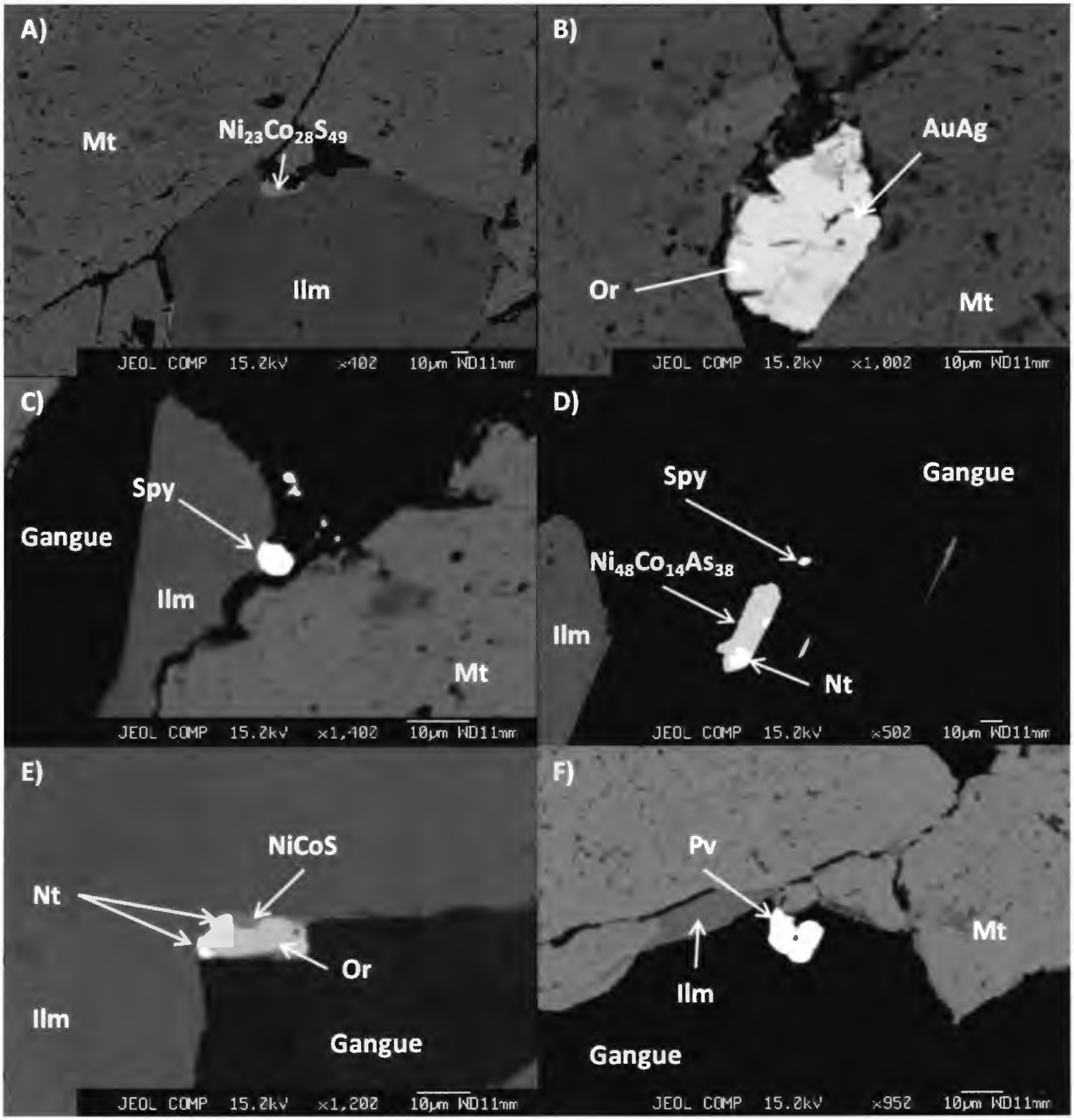

Figure 3.11: Late Pt mineralization seen in C, D, E & F. Sulphides and arsenides also form late with respect to magnetite and ilmenite (A & B). (FGA58-140.40m)

FGA61-76.20m

Table 3.12 Sample FGA61 76.20 mineralogy.

Mineral	*Chemical Formula*	*Number of Mineral Grains found*	*Average Size (μm)*
Magnetite	Fe_2O_3	Abundant	
Ilmenite	$FeTiO_3$	Abundant	
Chalcopyrite	$CuFeS_2$	1	10
Sphalerite	ZnS	2	10
NiCoS		1	40
Co-rich Pentlandite	$(Fe,Ni)_9S_8$	1	20
$Ni_{93}Fe_5P_2$		1	12
Sperrylite	$PtAs_2$	3	2-20

Fe-Oxides

Magnetite and ilmenite account for only 46% modal rock volume of this sample. This is quite different from other samples in which they are usually above 80% combined. Hornblende, biotite, and chlorite account for 52% total rock volume. Ilmenite grains show two distinct textural features. Ilmenite grains associated with secondary silicates, form 0.2 mm rounded inclusions, while ilmenite grains associated with magnetite form sub to euhedral grains. Magnetite grains are anhedral and highly fractured when in contact with silicates. Occasionally, magnetite grains display ilmenite exsolution lamellae at a 60°/120° orientation.

Sulphides

Chalcopyrite, sphalerite, NiCoS and co-rich pentlandite are present in this sample. Chalcopyrite forms an anhedral 10 μm grain, located at the boundary between magnetite and a gangue mineral. Sphalerite forms small, 10μm inclusions within magnetite. NiCoS is found as a 40 μm subhedral grain, intergrown with gangue mineralization, present in interstitial space. Pentlandite forms a 20 μm subhedral inclusion within magnetite. Gangue mineralization is located near the border of the inclusion.

Ni-Alloy

NiFeP is present in the slide as a subhedral 12 μm inclusion within ilmenite (Fig, 3.12C).

Platinum Group Minerals

Sperrylite is abundant as both small and large inclusions. Sperrylite is found as a small (2μm), anhedral inclusion within gangue mineralization near the grain boundary with a corresponding ilmenite crystal (Fig, 3.12B). Two grains of sperrylite are present as inclusions within ilmenite (Fig, 3.12A). Both show an anhedral shape, but vary in size (2μm & 20μm).

Crystallization Sequence

I. **Mt-Ilm-NiFeP-Spy(early)-Sph-Pl**

II. **Spy(late)**

III. **Gangue minerals-Cpy-NiCoS**

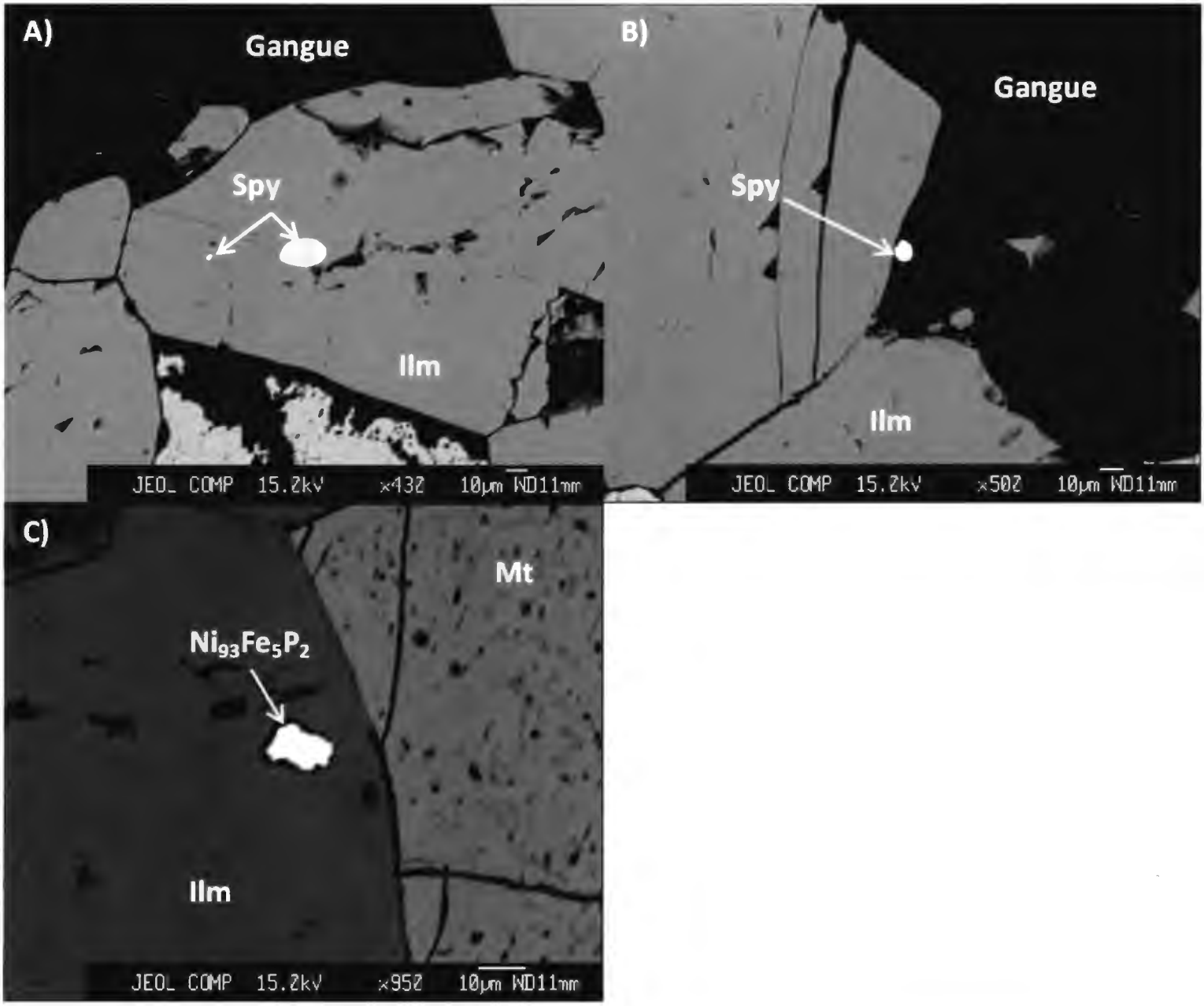

Figure 3.12: Early Pt-mineralization (A) and later Pt-mineralization (B) are both found in this sample. (FGA61-76.20m)

FGA69-45.52m

Table 3.13 Sample FGA69 45.52 mineralogy.

Mineral	*Chemical Formula*	*Number of Mineral Grains found*	*Average Size (μm)*
Magnetite	Fe_2O_3	Abundant	
Ilmenite	$FeTiO_3$	Abundant	
Chalcopyrite	$CuFeS_2$	4	15-40
Chalcocite	Cu_2S	1	30
Pyrite	FeS_2	2	40-100
Co-rich Pentlandite	$(Fe,Ni)_9S_8$	2	20
Sperrylite	$PtAs_2$	4	1-8
Tetraferroplatinum	PtFe	1	5
$Pd_{78}Sb_{22}$		1	1

Fe-Oxides

Magnetite and ilmenite are the most abundant ore minerals, forming cumulus phases. Ilmenite grains occur as rounded inclusions in silicate minerals, and as sub-rounded grains forming sharp contacts with magnetite grains. Grains are on average 0.2 mm in size. Magnetite is found as coarse grained (>1.0 mm) euhedral crystals, accounting for the majority of minerals present in the slide.

Sulphides

Chalcopyrite, chalcocite, pyrite, and cobalt-rich pentlandite are present in this sample. Sulphides are found in clusters, located in the interstitial space between primary magnetite and ilmenite grains. Chalcopyrite is forms large (40μm), anhedral grains in a sulphide aggregate (Fig, 3.13C). A smaller (15μm) grain of chalcopyrite is present as an inclusion within ilmenite. A single chalcocite grain is found in interstitial space, forming a sharp boundary with pyrite (Fig, 3.13A). The chalcocite grain is anhedral and 30 μm in size. Pyrite is present twice as large (40-

100μm) anhedral grains located in sulphide clusters (Fig, 3.13A,C). Cobalt-rich pentlandite is often associated with pyrite and chalcopyrite, occurring as 20 μm subhedral grains (Fig, 3.13B,C).

Arsenides

No arsenides were present in this slide other than those associated with PGMs.

Platinum Group Minerals

Platinum minerals form small deformed blebs, found primarily as inclusions within magnetite. Sperrylite grains range from 1 to 8 μm and occur occasionally with gangue mineral halos (Fig, 3.13F). Sperrylite is also found as a small anhedral grain at the boundary between magnetite and gangue mineralization (Fig 3.13E). Tetraferroplatinum forms a 5 μm inclusion within magnetite. One PdSb (1μm) grain, likely stibiopalladinite was found at the boundary between magnetite and a sulphide aggregate (Fig, 3.13C).

Crystallization sequence:

I. **Mt-Ilm-Spy-Tp**

II. **PdSb-Cpy-Py-Ch-Pl**

III. **Gangue minerals**

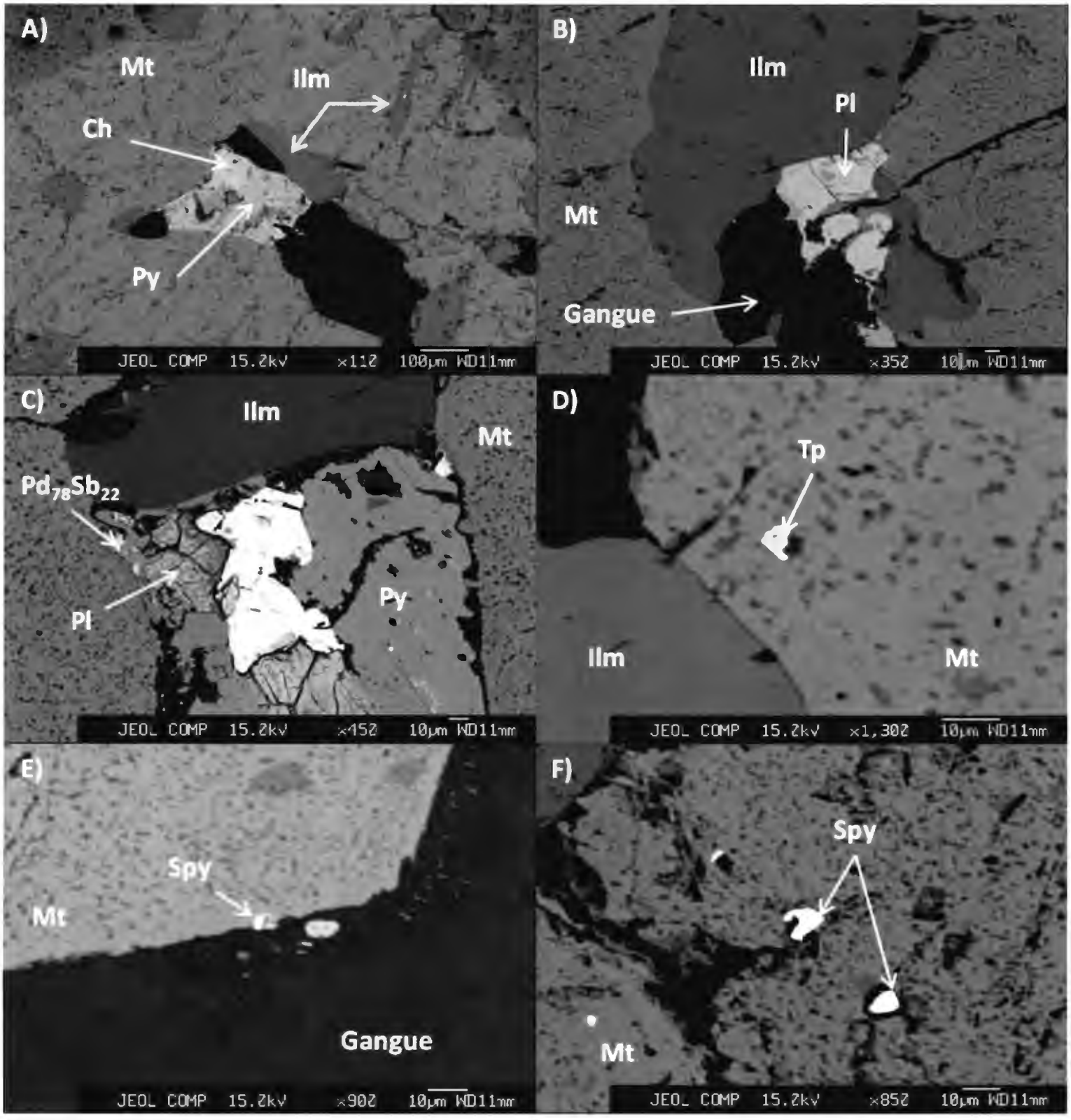

Figure 3.13: Sulphides present in clusters (A & B). Early Pt-mineralization found in photomicrographs D & E. Sulphide cluster present in photo (C). (FGA69 45.42m)

3.3 Summary of Results

3.3.1 Fe-Oxides

Magnetite and ilmenite account for the majority of the modal rock volume, generally occupying 90% of the slide. The other 10% is composed of silicates, and minor (1%) sulphides, arsenides, bismuthides, antimonides and alloys. Metamorphic silicates form aggregates of tremolite, hornblende, chlorite, actinolite and serpentine, with minor primary pyroxene and olivine. Magnetite is the predominant phase, accounting for 60% modal rock volume, followed by ilmenite occupying 30%. Two separate phases of magnetite are often present, one displaying exsolution lamellae of ilmenite, the other composed of finer grained magnetite with anhedral ilmenite inclusions. Magnetite generally forms euhedral cumulus phases, ranging from 0.3 to 2.0 mm in size, while ilmenite forms subhedral to anhedral crystals, ranging from 0.2 to 1.0 mm in size. Annealing textures, distinguished by 120° grain contacts, are often present, probably caused by the late metamorphic event. This texture has important implications with regards to PGM crystallization. PGE inclusions could be later intergrain phases encapsulated by large, re-crystallized grains formed during metamorphism.

3.3.2 Sulphides

Base metal sulphides (BMS) are present in all slides, with cobalt-rich pentlandite being the most abundant phase, followed by NiCoS, chalcopyrite, and sphalerite. Minor amounts of pyrite, galena, NiCuFeS, cobaltite, CuNiCoS, chalcocite, and NiS are also present. Sulphides generally form clusters within interstitial space. Rarely, locally minute sulphide inclusions are present in magnetite and ilmenite. Chalcopyrite occasionally forms zoned crystals with chalcocite rims. Sulphides are commonly subhedral to anhedral, ranging in size from 10μm to 150μm. Early galena, sphalerite and pyrite are found as inclusions within chalcopyrite (Fig. 3.3). A proposed

crystallization sequence for sulphides is developed; galena, pyrite, and sphalerite, followed by later chalcopyrite, pentlandite, NiCoS, NiS, NiCuFeS, and chalcocite.

3.3.3 Precious & Base Metal Alloys

Various Au, Ni and Cu alloys are present in minor amounts within the slides studied. Au is present as electrum and as a gold arsenic complex. Both phases are present as minute inclusions within magnetite and ilmenite (Fig. 3.1). NiFe alloys are located at grain boundaries forming small (10μm) sub-rounded grains (Fig. 3.9). NiSb is found as an inclusion within a larger NiCoAs host (Fig 3.5).

3.3.4 Platinum Group Minerals

The most abundant PGM is sperrylite followed by tetraferroplatinum. Platinum minerals occur predominantly (86% of the time) as inclusions within magnetite and ilmenite, and rarely as inclusions within silicate minerals. Palladium minerals are found primarily (90% of the time) as inclusions within metamorphic silicates, forming complexes with Te, Bi and Sb. PGMs form as small (5-10μm) anhedral blebs, with the exception of one sperrylite grain (120μm).

PGMs and sulphides do not account for a large percent of the total modal rock volume. Generally sulphides and PGMs account for 1% or less of the total rock volume, with Pt & Pd values ranging between 0.1-6.0 g/tonne.

Table 3.14: Ore phases present in the 13 thin sections studied.

Sample		FGA 69	FGA03	FGA14	FGA80	FGA43	FGA20	FGA20	FGA58	FGA23	FGA61	FGA 07	FGA04	FGA17
Drill core (meters)		45.52	42.27	22.9	22.52	104.68	53.88	52.72	140.4	49.8	76.2	52.18	45.52	82.24
Fe-Oxides														
Magnetite		x	x	x	x	x	x	x	x	x	x	x	x	x
Ilmenite		x	x	x	x	x	x	x	x	x	x	x	x	x
Sulphides														
Chalcopyrite		x		x	x						x	x		
Chalcocite					x	x								
Pyrite		x								x		x		
Sphalerite					x			x	x	x	x	x		
Galena										x		x		
CuNiCoS	(28:31:14:27)Fletcherite		x											
Cobaltite					x									
NiFeS	(33:19:48) Pentlandite	x					x					x		
NiCuFeS	(16:17:20:46) Samaniite											x		
NiS	(69:31) Heazlewoodite						x							
NiCoS	(39:36:25) Siegenite		x		x		x	x	x		x	x	x	x
Pentlandite	(18:7:26:49) Co-rich Pentlandite	x		x		x		x	x		x	x	x	x
Cu & Cu-alloys														
Native copper				x										
CuZnFe	(64:23:13) Zhanghengite								x	x			x	
CuFe				x										x
Ni-alloys														
NiSb	(46:54) Breithaupite					x								x
NiCoAs						x		x	x			x		x
NiFe	(92:8)									x				
Orcelite	Ni5As2						x		x			x	x	x
Krutovite	NiAs2							x						
Dienerite	Ni3As		x					x		x				
NiFeP	Melliniite										x			x
Gold & Silver														
AuAg	(74:26) Petrovskaite				x				x					
AuAs	(42:58)		x				x							
Pt-minerals														
Sperrylite		x	x		x		x	x	x		x	x		
Tetraferroplatinum		x	x				x					x	x	
PtSn	Nigglite								x					
PtAsFeNi										x			x	
PtNiFe	Ferronickelplatinum							x						
PtPdSnCu	(18:41:29:12)						x		x					

PtSbSnNiCoS														x
Pd-minerals														
PdBiTe	(32:37:42) Kotulskite				x									
PdBiSb			x		x									
PdBi			x											
PdSb	Stibiopalladinite	x	x											
PdSn	(65:28) Paolovite								x					

3.5 Geochemistry

Trace element geochemistry demonstrates similar patterns for most trace elements regardless of the different rock types present in the intrusion. Figure 3.15 shows geochemical variation with respect to the standard chrondrite. Pegmatite samples are enriched in Large Ion Lithophile (LILE) elements (Rb, Th, and Ta) with respect to the other lithologies. However, they are similarly enriched in High Field Strength (HFS) elements (Hf, Y, and Lu). Gabbro, pyroxenite and magnetite-pyroxenite show fairly similar trace element patterns. Gabbro is slightly more enriched than magnetite-pyroxenite followed by pyroxenite. Magnetite rich samples are strongly depleted in trace elements compared to the previous four lithologies. However, titanium is enriched in magnetite samples, for two possible reasons. Magnetite can incorporate up to 5% TiO_2 within its crystal structure and magnetite samples generally contain a high proportion of ilmenite.

The extent of fractionation determines the enrichment of incompatible elements. In a fractionation series, ranging from ultramafic to felsic, we would expect a low to high abundance of incompatible elements respectively. Comparing PGE-rich magnetite to PGE-poor magnetite provides an interesting pattern. Figure 3.14 highlights that PGE-rich magnetite has a slightly different trace element pattern compared to PGE-poor magnetite ore. It also shows depletion in copper compared to the regular magnetite samples. This trend was recognized by Keays (2007) and is used as an exploration target for locating PGE-rich zones at Maracas.

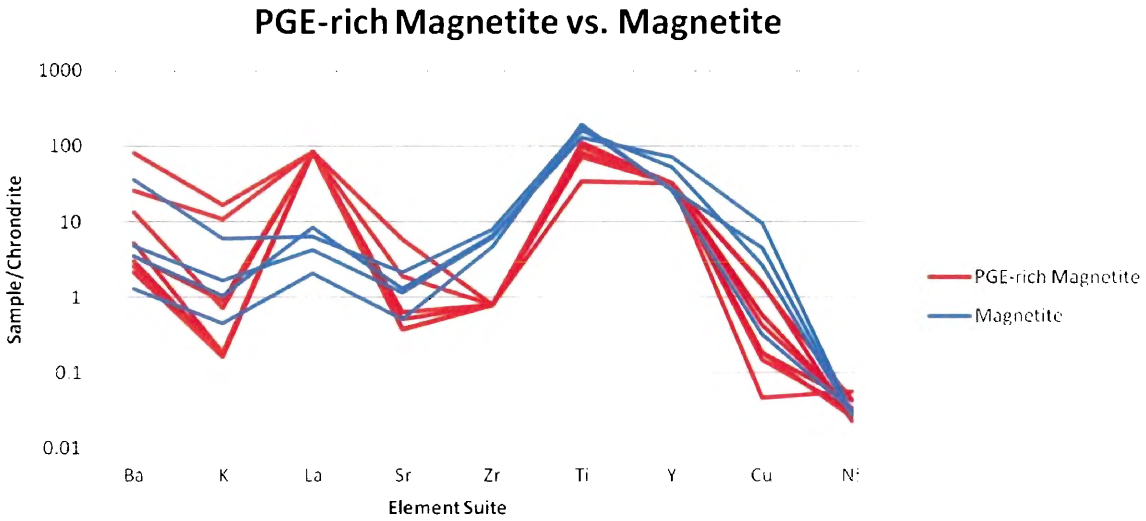

Figure 3.14 Trace element data comparing PGE-rich magnetite to regular magnetite samples (chrondrite values from McDonough & Suns, 1995)(www.earthref.org).

3.6 Microprobe Analyses

Microprobe analyses performed on five Pt-grains distinguished two separate platinum phases (sperrylite and tetraferroplatinum). Three grains from the FGA61 slide were determined to be sperrylite ($PtAs_2$). All three of these grains contain minor amounts of Au, Ni, Fe and Sb. The samples from FGA07 and FGA04 represent tetraferroplatinum (PtFe) with minor amounts of Au, Ni and Cu.

Table 3.15 Electron Microprobe data for Pt-minerals.

	FGA07	*FGA04*	*FGA61*	*FGA61(2)*	*FGA61(3)*
Te	0.1	0.05	0	0	0
As	0	0.06	40.37	40.04	39.98
Al	0.27	0	0	0	0
Ir	0.35	0.15	0	0	0
Au	3.72	4.97	3.48	3.67	3.57
Pd	0	0.01	0.06	0	0
Mg	0.15	0	0	0	0
Pt	63.83	71.43	50.47	53.25	52.04
S	0.07	0	0.06	0.06	0.29
Fe	27.18	21.13	1.96	0.81	1.89
Hg	0	0	0	0	0.05
Ru	0	0	0	0.01	0.12
Co	0.33	0.42	0.05	0.02	0.02
Pb	0	0.06	0	0.09	0
Sb	0	0	1.19	1.04	3.02
Ni	2.38	2.48	0	0.02	0.03
Ag	0	0	0	0.01	0
Cu	1.11	0.35	0	0	0
Rh	0.38	0.31	0.23	0.21	0.65
V	0.44	0.04	0	0.02	0.13
Ti	0.13	0.89	0.41	0.25	0
Total	100.43	102.33	98.29	99.49	101.78

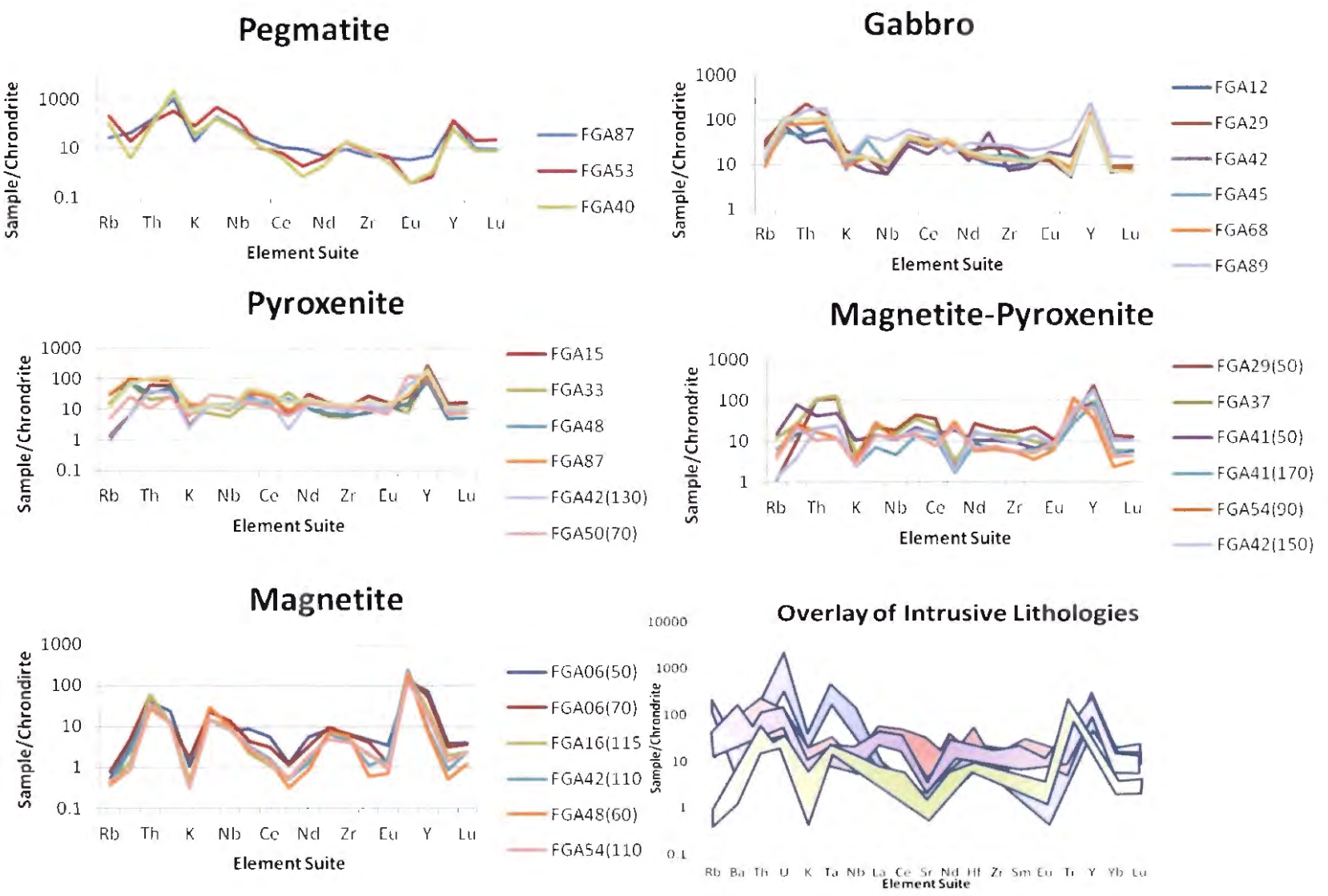

Figure 3.15 Trace Element data for each lithology, normalized to chrondrite values (McDonough & Suns, 1995) (www.earthref.org). Trace element data taken from GEOSOL Labs, Belo Horizonte, Brazil.

Chapter 4: Discussion

4.1 Comparison to Previous work

Previous work done by Sá et al. (2005) was similar to the findings of this study. Both studies found cobalt- rich pentlandite and chalcopyrite to be the predominant sulphide phases with minor amounts of chalcocite, pyrite, galena, and sphalerite. The size and location of sulphides also correlates well with previous findings. Sá et al. (2005) determined the origin of PGE mineralization to be orthomagmatic, which we believe is the main mechanism of mineralization. Within the confines of this study, NiCoS appears to be an abundant sulphide and is not mentioned explicitly by Sá et al. With respect to sperrylite, the findings of Sá et al (2005) differ. In the present study, sperrylite is predominantly found as inclusions within magnetite and ilmenite, whereas in the previous work, sperrylite was found mainly within altered silicates.

The previous work done by Brito et al. is more aligned with results found in this study. Brito et al. also found that the majority of sperrylite grains were present as inclusions within magnetite, compared to inclusions found in silicates. The three textural features outlined in section 2.6, described by Brito et al., were also confirmed in this study. Furthermore, the authors recognised the relationship between both primary (orthomagmatic) and secondary (hydrothermal/metamorphic) PGE phases.

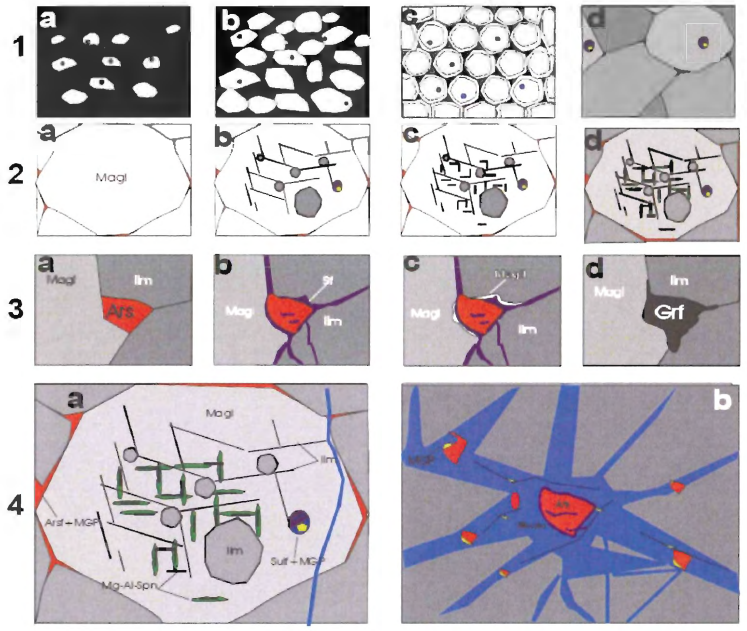

Figure 4.1: A schematic crystallization diagram created by Brito et al. (n.d.). Numbers one through four demonstrate the sequence of mineralization within the intrusion. Early PGE mineralization associated with Mt formation (1). Followed by later interstitial sulphide and arsenides (3). Finally, late stage metamorphic/hydrothermal generation of PGE's within fractured interstitial space (4).

4.2 Variation in Ore Mineralogy

The results obtained from the Electron Microprobe (EMP) indicate some mineralogical variation between samples. Samples FGA03, FGA58, FGA69 and FGA80 were the only samples in which palladium (Pd) minerals were found. These samples geochemically ranged from 35-1106 ppb Pd respectively. There does seem to be an inverse correlation between Pd-minerals and arsenide minerals. Three out of the four slides containing palladium minerals are depleted in arsenides. This indicates that Pd-minerals crystallized at conditions where arsenic does not reach saturation. The location of Pd-minerals, predominantly as inclusions within gangue minerals, suggests that they formed during the late stages of magma crystallization, possibly during recrystallization/remobilization. The compositions of Pd-minerals (PdBi, PdBiTe, PdSb, PdBiSb and PdSn) may provide an indication of the temperature of formation. A study done by Evstigneeva (1993) indicated that the refractory PGE phase PdSn could crystallize

from chlorine bearing solutions at 300-400°C. Experimental systems have also been developed incorporating PGE's with Cl, Na, K, As, Sn, Sb, Bi, Pb and Te, in which most PGMs formed at temperatures between 240-500°C (Evstigneeva, 1993). Work done by Evstigneeva & Tarkian (1996) provides experimental results indicating that PGE sulphides subjected to chlorine-rich fluids containing Pb, Bi, Sb, As and Te will form low-temperature PGM alloys. This provides intriguing evidence supporting remobilization of PGMs according to the hydrothermal model.

Platinum mineralization predominantly forms arsenides, and Pt-minerals are often associated with Ni-arsenides. The dominant phase of platinum mineralization is sperrylite ($PtAs_2$). Pt-minerals are found predominantly as inclusions within primary ilmenite and magnetite grains. This mineral association suggests an early crystallization phase that indicates an orthomagmatic origin of Pt-mineralization. In this model, primary PGE's are expected to be associated with primary oxides, sulphides and silicates. Sperrylite, traditionally interpreted as a high-temperature magmatic mineral, has been experimentally synthesized from the combination of H_2PtCl_6 solution and As_2O_3 indicating that it could also be formed by hydrothermal processes (Evstigneeva & Tarkian, 1996). This indicates that the location and association of sperrylite with adjacent minerals is crucial to determining whether it formed through primary or secondary magmatic processes.

PGMs are almost exclusively located within the Gulcari A magnetite deposit. There does not appear to be any correlation between location within the deposit and average grade of Pt and Pd. It is possible that samples near the base of the horizon show slightly higher PGE values than the samples taken near the top of the magnetite horizon. More samples throughout the magnetite horizon would be necessary to test this observation. Sulphide abundance and phases present are fairly constant throughout a vertical profile of the magnetite pod. However, in section 6175

represented by slides FGA58, FGA43, FGA23, FGA69 and FGA03 are concentrated in proximity, PGE's and sulphides.

No PGE sulphides were found in the studied samples. The small modal abundance of base metal sulphides (BMS) along with the lack of PGM sulphides indicates that primitive magma source was relatively sulphur-poor. Although this does not correlate well with the model of an immiscible sulphide fluid entraining PGE's, it does not negate the model entirely. The abundant fractionation (60%) necessary to crystallize magnetite may have caused a delay in sulphur saturation (Sá et al., 2005). An abundance of Fe-oxides allowed for sulphur saturation of a sulphur poor magma. Once the sulphide fluid separated from the siliceous melt, it could still partition PGE's effectively.

The variation in PGE mineralogy suggests two stages of PGM development. The first consisted of an early magmatic sequence composed of dominantly Pt-minerals that formed inclusions within magnetite and ilmenite. Following early mineralization was a late stage, hydrothermal/remobilizing sequence. This sequence, composed predominantly of Pd-minerals, formed likely during metamorphism where fluid was present. The minimal presence of Pd-minerals in metamorphic silicates indicates the remobilization/crystallization of later PGE's was minor in comparison to orthomagmatic mineralization.

4.3 Textural Implications

The textures observed under reflected light and in back scatter electron images provide detailed insight into the crystallization processes. Ilmenite exsolution lamellae inside magnetite are typical features present in oxides formed by primary igneous crystallization (Fig. 4.1). Magnetite and ilmenite grains spatially close to exsolution lamellae form subhedral to euhedral coarse cumulus phases, with sharp grain-boundary contacts. In other areas, magnetite near grain-

boundary contacts display resorption and annealing textures. The two textures present indicate two different styles of crystallization. The exsolution lamellae likely formed during the cooling and unmixing of a primary solid solution, whereas the resorption and annealing textures are interpreted to have formed during recrystallization, locally incorporating earlier mineral phases along the boundaries of annealing grains. Grain size and textures are confined to specific domains within the samples analysed, indicating different degrees of recrystallization within the intrusion (Figure 4.1). Textural implications provide further evidence for a primary (orthomagmatic) and secondary (hydrothermal-metamorphic) crystallization.

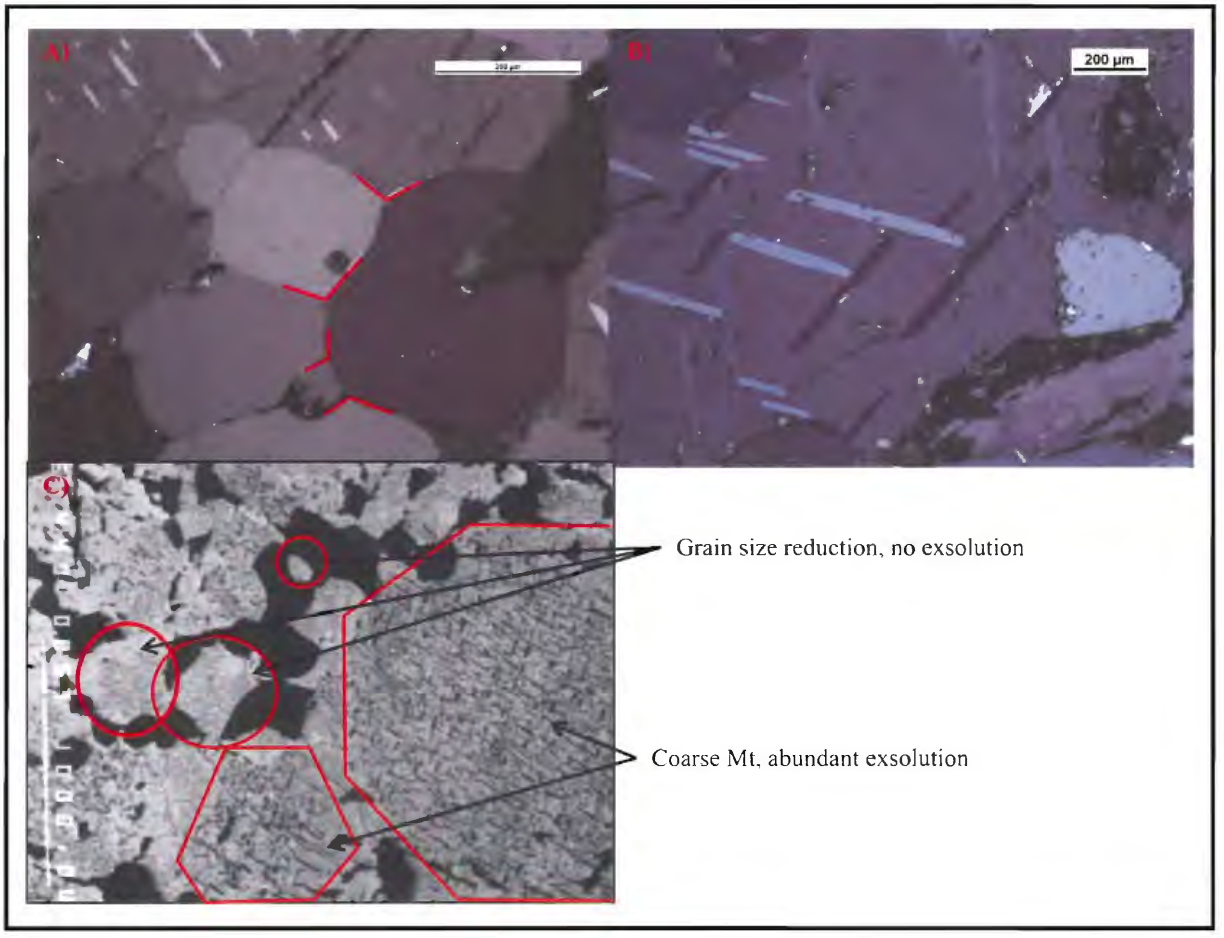

Figure 4.2 A) Granoblastic texture present between Mt and Ilm. B) exsolution lamellae at a 60°/120° orientation. C) Zones of primary crystallization beside a zone of grain size reduction.

4.4 Orthomagmatic Origin

The growth of chromite grains within a basaltic melt creates conditions where locally a reduction in fO_2 occurs along the crystal-melt interface (Mungall, 2005). A sufficient reduction in fO_2 sufficiently causes alloy saturation, allowing chromite grains to overgrow the PGMs. The bulk physical and chemical similarities between chromium and vanadium (Table 4.1) suggest that, in the case of the Rio Jacaré, vanadium-rich magnetite collected PGMs in a similar fashion to chromite within the more famous layered mafic intrusions.

Table 4.1 Physical properties of vanadium and chromium.

	Vanadium	Chromium
Atomic Radius (Pico meters)	134	128
Atomic Weight	51.996	50.94
Valence States	5, 4, 3, 2, 1	6, 5 , 4 , 3 , 2 , 1
Melting Temperature (° C)	1910	1907

The Baula Complex in India provides an interesting example of a LMI containing both magmatic and hydrothermal PGE mineralization. Within the weakly altered to unaltered layers of the chromite-rich Bangur gabbro, PGMs are present as inclusions within unaltered magmatic silicates (Augé et al., 2002). Magmatic PGE mineralization is elevated in platinum and has a high Pt/Pd ratio. PGMs present in this portion of the intrusion are dominated by malanite ($Cu(Pt,Ir)2S_4$), sperrylite ($PtAs_2$) and isoferroplatinum (Pt_3Fe). The Rio Jacaré also displays elevated Pt with a high Pt/Pd ratio, along with abundant sperrylite.

Applying the orthomagmatic model to the Rio Jacaré provides a unique set of limitations. The metamorphic overprint present throughout the intrusion requires revision to a purely magmatic

model. Subsequent alteration of PGMs is likely, with a high remobilization potential. Theoretically, any PGMs present in relict pyroxene would have been remobilized during its alteration to amphibole. However, the presence of high temperature sperrylite, and inclusions of PGM in magnetite and Ni-arsendies, reflect orthomagmatic generation of PGMs.

4.5 Hydrothermal Origin

The Merensky and J-M reefs, of the Bushveld and Stillwater intrusions respectively, are thought to represent hydrothermal enrichment of platinum and palladium. The Merensky reef and the Rio Jacaré show similarities in sulphide and PGM mineralogy. At the Western Platinum mine, Bushveld Complex, sperrylite is the most abundant platinum mineral (Brynard et al., 1976). Pt-Fe alloys, stibiopalladinite and minor kotulskite are also present in both intrusions. Sulphides found at the Western Platinum portion of the Merensky reef are pyrrhotite, pentlandite, chalcopyrite and pyrite in relative order of abundance. Although the Rio Jacaré does not show the same mineralogical abundances, similar sulphide phases are associated with LMI's. Retrogressive alteration silicates such as serpentine, biotite, and talc are also present at both localities. While mineralogical comparisons between the two deposits may be similar, the location of PGMs is substantially different. Within the Merensky Reef 84% of PGMs are found associated with base metal sulphides (Mostert et al., 1982). Furthermore, the majority of PGMs associated with base metal sulphides are found as inclusions or at the grain-boundary margin. In the Rio Jacaré, the majority of PGMs are found as inclusions within magnetite and ilmenite.

The J-M Reef within the Stillwater Complex represents another potential analog to mineralization in the Rio Jacaré. Platinum group mineralogy within the J-M Reef is dominated by Pt-Pd sulphides, followed by Pt-Fe alloys, Pd-Pt tellurides and other minor Pd-rich phases

(Godel & Barnes, 2008). The Gulcari A deposit is composed predominantly of Pt-arsenides, Pt-Fe alloys, Pt-Pd tin phases, and minor Pt-Pd alloys. Due to late metamorphic events, the J-M Reef and Rio Jacaré contain similar metamorphic silicates (chlorite and tremolite-actinolite).

The Merensky Reef and the J-M Reef show a strong correlation of PGE mineralization associated with base metal sulphides. PGMs are found predominantly on the boundary of sulphide grains or as inclusions (Godel & Barnes, 2008).

The 2.4 Ga Imandra layered igneous complex hosts PGMs with a distinctly hydrothermal signature. Within the layered intrusion PGMs occur as minute grains associated with hydrous silicates, chromite and base metal sulphides (Barkov & Fleet, 2004). PGMs present in chromites are almost all sulphides or sulfarsenides. The small grain size and minimal presence of base metal sulphides indicates that the crystallizing magma was relatively sulphur-poor. PGE mineralization is predominantly found in the hydrous silicates, hornblende, edenite, talc and phlogopite (Barkov & Fleet, 2004). Chlorine is evident in the system, determined by its high concentration in apatite grains. Although the Rio Jacaré intrusion shares similar mineralogy, with abundant sperrylite and the presence of hornblende and phlogopite, predominant PGE mineralization is located in magnetite and ilmenite, not hydrous silicates. The Imandra Complex also hosts PGE sulphides which are not found in the Rio Jacaré.

Traditionally, the hydrothermal model has been used to describe the enrichment of PGMs during a late magmatic/hydrothermal event. In the case of the Rio Jacaré, it is more likely that hydrothermal fluids, a consequence of metamorphism, were responsible for remobilizing pre-existing PGMs. It is clear, from the significant generation of hydrous amphiboles, that a fluid was present during metamorphism. Whether it was Cl^- rich or not has yet to be determined.

There is sufficient evidence to suggest that some Pd-minerals were remobilized due to their presence in metamorphic minerals, while Pt-minerals were relatively stable.

4.6 Geochemistry

Trace element geochemistry plotted against standard chrondrite values can be used to help infer a crystallization sequence for the intrusion. Each lithological unit within the intrusion occupies a characteristic "field" of values. Pegmatite values are, overall, enriched in incompatible elements compared to gabbro, which is enriched compared to magnetite. An understanding of crystal fractionation suggests the early crystallization of magnetite (depleted in incompatibles) versus the later crystallization of pyroxenite, gabbro and pegmatite (enriched in incompatibles with respect to magnetite). This correlates well with the idea that compatible (ultramafic to mafic) suites will crystallize first, lower in the intrusion compared to the more felsic counterparts (gabbro).

4.7 Economic Potential

Currently, the grades and gross tonnage of PGM ore at Maracas are not sufficient to allow for economic extraction. However, separating the PGM concentrate from V-rich magnetite ore may sufficiently enrich PGMs to economic levels. Largo plans to be extracting vanadium by the summer of 2013. V-rich magnetite will be extracted from the Gulcari "A" magnetite deposit, the same deposit that contains elevated PGE's. After the ore is crushed it will then be put through a magnetic separator. This separation effectively concentrates both vanadium and PGE's. The non-magnetic portion of the ore will become an enriched PGE concentrate that could elevate the Pt and Pd levels to economic grades.

4.8 Conclusion

Thorough analyses of electron microprobe data, PGM mineralogy, and ore textures suggest a two event mineralization sequence. An early crystallization event was responsible for crystallizing Pt-minerals, which formed inclusions within magnetite and ilmenite. This sequence was followed by a later hydrothermal or metamorphic event that crystallized PGMs consisting of Pt-alloys, Pd- bismuthides, tellurides, and antimonides located at the grain-boundary between Fe-oxides and silicates, or as inclusions within hydrous silicates. Work done by Armitage et al, (2002) indicates that (Pt, Pd) tellurides and antimonides form at lower temperatures relative to sperrylite. Although this does not confirm that the mineralization must be secondary, or possibly related to hydrothermal processes that occurred during metamorphism, it is in accord with known hydrothermal temperatures. Mineralization was likely formed prior to metamorphism, with late-stage fluids causing minimal remobilization of PGMs. Pd is more mobile than Pt under hydrothermal conditions. Evidence from BSE images supports the idea that remobilization of Pd-minerals occurred.

Two sets of separate evidence suggest that two different processes may have occurred during the life span of the Rio Jacaré. Firstly, the different positions of Pt and Pd minerals respectively, suggests that Pt minerals formed first, with Pd minerals forming later. Pt minerals are found as inclusions within magnetite and ilmenite, while Pd minerals are found primarily as inclusions within metamorphic silicates. Secondly, there is a distinct contrast between the mineralogy of Pt and Pd minerals. Pt minerals primarily form arsenides and Fe-alloys. Pd minerals on the other hand form bismuthide, telluride, and antimonide complexes. The contrasting positions and mineralogy of Pt and Pd minerals, provide strong evidence to support a two stage process of mineralization.

Chapter 5

5.1 Future Work

This study has presented evidence to suggest that two separate events were responsible for the enrichment and mobilization of platinum group elements. Research has been done to relate the Rio Jacaré to other LMI's sharing similar mineralogical and tectonic histories. In reality, the Rio Jacaré appears to be a unique occurrence of elevated PGE's associated with Fe-Ti-V oxides. However, no work yet has been done to analyse the extent, or the mechanism, of potential hydrothermal PGE occurrences. In order to accurately assess the importance of second-stage alteration, fluid inclusion work should be done on PGMs associated with alteration silicates. It would also be interesting to investigate the chlorine content of secondary silicates.

With respect to metamorphism, no detailed study has been done to investigate peak metamorphic pressure, temperature and related metamorphic minerals. A better understanding of the Rio Jacaré's deformation history would help to thoroughly understand the genesis of PGE mineralization.

No, detailed work has yet been done on the Gulcari "B" and Novo Amparo magnetite deposits located in the Rio Jacaré. Both zones contain elevated levels of PGE's in similar abundances to Gulcari A. A better understanding of these PGE occurrences could provide further insight into the extent and style of mineralization. Lastly, it would be interesting to analyse pentlandite to see if it includes trace amounts of Pt and Pd within its crystal structure. Previous studies (Gervilla & Kojonen, 2002) have found that pentlandite, where abundant, can accommodate sufficient levels of Pt (42 ppm) and Pd (16-150 ppm) within its crystal structure. This would be particularly interesting for the slide FGA43 104.68 which assayed 4235ppb Pt and 105ppb Pd but for which no platinum group minerals were found during EMP analyses.

References

Armitage, P., McDonald, I., Edwards, S., & Manby, G. (2002). Platinum-group element mineralization in the Platreef and calc-silicate footwall at Sandsloot, Potgietersrus District, South Africa. *Applied Earth Science* , 36-45.

Auge, T., Salpeteur, I., Mukherjee, M., & Patra, R. (2002). Magmatic and Hydrothermal Platinum-Group Minerals and Base Metal Sulfides in the Baula Complex, India. *The Canadian Mineralogist , 40*, 277-309.

Barkov, A., & Fleet, M. (2004). An Unusual Association of Hydrothermal Platinum-Group Minerals from the Imandra Layered Complex, Kola Peninsula, Northwestern Russia. *The Canadian Mineralogist* , 455-467.

Barkov, A., Fleet, M., Martin, R., & Halkoaho, T. (2005). New Data on "Bonanza"-Type PGE Mineralization in the Kirakkajuppura PGE Deposit, Penikat Layered Complex, Finland. *The Canadian Mineralogist* , 1663-1686.

Boudreau, A., & McCallum, I. (1992). Concentration of Platinum-Group Elements by Magmatic Fluids in Layered Intrusions. *Economic Geology , 87*, 1830-1848.

Brito, R., Nilson, A., & Laflame, G. (n.d.). PGM and Complex Ni-Fe-Cu-Co Arsenide-Sulfide Paragenesis Associated with Fe-Ti-V Oxides of the Gulcari Magnetite Pod, Rio Jacare Sill, Bahia, Brazil.

Brynard, H., De Villiers, J., & Viljoen, E. (1976). A mineralogical Investigation of the Merensky Reef at the Western Platinum Mine, near Marikana, South Africa. *Economic Geology* , 1299-1307.

Evstigneeva, T. (1993). Platinum-group minerals- and sulphide-paragenesis in massive Cu-Ni ores. *IAGOD Symposium on Mineralization connected with mafic and ultramafic rocks.* New Orleans.

Evstigneeva, T., & Tarkian, M. (1996). Sythesis of platinum-group minerals under hydrothermal conditions. *European Journal of Mineralogy , 8*, 549-564.

Freil, J. J. (1998). *X-Ray and Image Analysis in Electron Microscopy.* Princeton, New Jersey, United States of America: Princeton Gamma-Tech Inc.

Geochemical Earth Reference Model. (n.d.). Retrieved from www.earthref.org

Gervilla, F., & Kojonen, K. (2002). The Platinum-Group Minerals in the Upper Section of the Keivitsansarvi Ni-Cu-PGE Deposit, Northern Finland. *The Canadian Mineralogist , 40*, 377-394.

Godel, B., & Barnes, S.-J. (2008). Image Analysis and Composition of Platinum-Group Minerals in the J-M Reef, Stillwater Complex. *Economic Geology* , 637-651.

Goodge, J. (2011, February 1). *Energy-Dispersive X-Ray Spectroscopy (EDS).* Retrieved November 11, 2011, from Geochemical Instrumentation and Analysis: http://serc.carleton.edu/research_education/geochemsheets/eds.html

Hanley, J. (2005). The Aqueous Geochemistry of the Platinum Group Elements (PGE) in Surficial, Low-T Hydrothermal and High-T Magmatic-Hydrothermal Environments. *Mineralogical Association of Canada*, (pp. 35-56). Oulu.

Keays, R. (2007). *Report on Maracas PGE-bearing Fe-Ti-V Deposit.* Toronto: Largo Resources.

Mostert, A., Hofmeyr, P., & Potgieter, G. (1982). The Platinum-Group Mineralogy of the Merensky Reef at the Impala Platinum Mines, Bophuthatswana. *Economic Geology* , 1385-1394.

Mountain, W. B., & Wood, A. S. (1988). Chemical Controls on the Solubility, Transport, and Deposition of Platinum and Palladium in Hydrothermal Solutions: A Thermodynamic Approach. *Economic Geology , 83*, 492-510.

Mungall, J. (2005). Magmatic Geochemistry of PGE. *Exploration for Platinum-Group Elements Deposits* (pp. 1-34). Oulu: Mineralogical Association of Canada.

Prendergast, M. (2000). Layering and Precious Metals Mineralization in the Rincon del Tigre Complex, Eastern Bolivia. *Economic Geology , 95*, 113-130.

Robb, L. (2005). *Introduction to Ore-Forming Processes.* Malden, Massachusettes, United States: Blackwell Publishing.

Sa, J., Barnes, S., Prichard, H., & Fisher, P. (2005). The Distrubution of Base Metals and Platinum-Group Elements in Magnetite and Its Host Rocks in the Rio Jacare Intrusion, Northeastern Brazil. *Economic Geology , 100*, 333-348.

Winter, D. J. (2010). *Principles of Igneous and Metamorphic Petrology* (2nd Edition ed.). Upper Saddle River, New Jersey, United States: Prentic Hall.

Appendix A

Table 3: A list of trace element geochemical data done by ACME Labs, Vancouver.

Sample #	Rock Type	Rb	Ba	Th	U	K	Ta	Nb	La	Ce	Sr	Nd	Hf	Zr	Sm	Eu	Ti	Y	Yb	Lu
FGA12(45)	Gabbro	62.2	264	1.4	0.5	7221	0.2	2.1	8.2	15.6	264.9	7.2	1.1	35.4	1.68	0.94	2400	10.7	1.09	0.18
FGA15(110)	Gabbro	7.2	34	2.2	1	2075	0.2	2.7	14.4	31.3	34.9	19.2	1.7	55.6	4.68	1.09	6780	28.7	2.55	0.39
FGA29(10)	Gabbro	76.4	223	6.6	1	11039	0.2	1.5	10.2	22	280.8	9	2.6	88.3	2.04	0.68	2520	13.6	1.41	0.23
FGA42(50)	Gabbro	52.5	163	0.9	0.3	6640	0.1	1.5	6.4	10.7	274.3	5.6	0.8	28.8	1.32	1.08	7020	10.2	1.17	0.19
FGA45(70)	Gabbro	26.8	122	1.3	0.6	4399	0.5	2.4	10.8	17.4	256.9	9.3	1.7	61.4	1.97	0.91	2580	12.2	1.31	0.19
FGA68(30)	Gabbro	20.7	178	2.4	0.7	5063	0.2	2.7	9.6	16.4	247.3	7.6	1.4	48.9	1.80	0.87	3600	12.4	1.41	0.19
FGA89(150)	Gabbro	34.9	213	4.8	1.5	6806.0	0.6	8.1	14.5	28.6	133.5	14.2	3.0	103.1	3.27	1.37	16620	22.4	2.44	0.37
FGA41(30)	Gabbro	2.7	16	0.9	0.3	1162	0.3	3.6	4.3	10.4	20.2	7.9	1.3	36	2.22	0.49	24780	16.9	1.65	0.26
FGA89(270)	Gabbro	44.6	255	3.1	0.9	8300.0	0.2	2.4	10.6	19.6	313	8.5	1.6	52.6	1.78	0.93	2700	11.5	1.18	0.17
FGA6(90)	Pyroxenite	2.6	15	0.2	0.2	1494	1	10	2.1	5.9	26.8	4.3	0.7	22	1.24	0.41	11400	9.2	0.98	0.16
FGA15(110)	Pyroxenite	2.9	15	1.7	0.5	1577	0.2	2.6	7.2	18.5	55.6	14.3	1.7	47.3	4.03	0.95	5820	25.6	2.47	0.39
FGA33(45)	Pyroxenite	33.1	157	0.6	0.2	4316	0.1	1.3	4.1	8.2	280.6	4.9	0.6	20	1.46	0.69	3240	11.2	1.07	0.18
FGA41(150)	Pyroxenite	1.9	3	0.2	0.1	249	0.1	0.6	1.5	2.3	5.5	2.2	0.5	13.1	0.67	0.25	15660	5.4	0.58	0.09
FGA48(120)	Pyroxenite	70.6	166	1	0.4	6972	0.2	3.4	5.8	9.5	176.1	4.8	0.8	23.9	1.18	0.59	6900	7.6	0.76	0.13
FGA87(60)	Pyroxenite	64.9	226	2.6	0.7	7968	0.2	2.2	9.1	14.4	70.8	7.3	1.3	46.9	1.63	0.68	10740	11.3	1.17	0.18
FGA42(130)	Pyroxenite	2.1	15	1.1	0.3	1328	0.2	2.5	4.9	11.3	17.7	7.3	1.2	33	1.98	0.55	25500	14.4	1.53	0.24
FGA50(70)	Pyroxenite	10.7	57	0.3	0.2	3403	0.4	5.9	3.7	6.9	46.6	6.9	1.4	43.1	1.51	0.38	54420	11.6	1.19	0.18
FGA68(61)	Pyroxenite	23.3	148	3.1	0.9	4731	0.2	2.9	11.7	20.3	126.7	10.0	1.6	53.3	2.69	0.79	14220	18.9	1.88	0.28
FGA29(30)	Mag-Pyx	91.6	375	1	0.5	11122	0.1	1.3	6.9	12.1	125.4	6.3	0.8	26.9	1.6	0.71	3960	12.4	1.15	0.18
FGA29(50)	Mag-Pyx	2.5	23	3.1	0.9	1660	0.3	4.5	10.6	22.5	16.1	12.8	2.1	65.3	3.34	0.61	17760	21.8	2.13	0.31
FGA37(150)	Mag-Pyx	27	60	3.3	1.1	2573	0.3	3.7	8.5	14.5	26.2	6.9	1.5	49.7	1.49	0.43	21660	9.3	0.96	0.14
FGA41(50)	Mag-Pyx	33.3	187	1.2	0.4	5810	0.2	2.6	5.3	9.4	145.6	4.8	1.1	35.4	1.05	0.56	29100	7.9	0.83	0.14
FGA41(170)	Mag-Pyx	14.3	35	0.6	0.2	1245	0.1	1.1	3.3	7.1	13.6	4.1	0.7	20.5	1.06	0.37	12600	7.8	0.82	0.15
FGA42(150)	Mag-Pyx	2.8	9	0.6	0.2	1245	0.2	2.8	4.4	10.1	14.8	8.2	1.3	34.9	2.21	0.46	21480	16.5	1.67	0.26
FGA50(110)	Mag-Pyx	8.4	55	0.3	0.1	1411	0.2	3	3.4	4.9	180.2	2.9	0.8	21.4	0.8	0.53	30240	6.1	0.65	0.11
FGA54(90)	Mag-Pyx	10.5	62	0.5	0.1	1992	0.4	2.9	3.6	4.6	247.3	2.7	0.7	20.6	0.55	0.35	51360	3.3	0.36	0.08

FGA68(210)	Mag-Pyx	0.7	4	0.2	0.1	249	0.2	2.2	1.3	2.9	6.7	2.5	0.7	17.6	0.86	0.19	51540	6.4	0.61	0.10
FGA06(50)	Magnetite	1.2	8	1.2	0.2	581	0.2	2	2	3.4	10.2	2.6	0.9	25.1	0.73	0.2	56580	6.7	0.63	0.1
FGA06(70)	Magnetite	1.7	11	1.7	0.1	913	0.3	3.3	1	1.9	9.1	1.5	1	23.3	0.63	0.07	70380	4.9	0.51	0.09
FGA16(115)	Magnetite	0.9	3	0.9	0.1	249	0.2	2.4	0.5	0.7	4.1	0.7	0.7	17.8	0.29	0.07	83940	2.4	0.31	0.06
FGA41(90)	Magnetite	128.2	82	0.4	0.3	3320	0.3	4.6	1.5	1.8	16.7	1.3	0.8	30.1	0.28	0.07	78720	2.5	0.31	0.05
FGA42(110)	Magnetite	0.9	6	0.9	0.1	166	0.2	2	0.8	1	4	0.6	0.7	17.7	0.17	0.09	108660	0.8	0.14	0.06
FGA48(60)	Magnetite	0.8	2	0.8	0.1	166	0.4	2.5	0.6	0.9	2.5	0.4	0.8	22.7	0.09	0.04	91440	0.7	0.08	0.03
FGA53(90)	Magnetite	0.4	1	0.4	0.1	83	0.1	0.5	0.3	0.1	0.8	0.3	0.5	14.5	0.06	0.02	94020	0.3	0.05	0.02
FGA54(110)	Magnetite	1	2	1	0.1	166	0.2	2.1	0.7	0.8	4.2	0.9	0.5	15.7	0.33	0.05	54600	1.7	0.22	0.06
FGA87(250)	Magnetite	2.1	2	2.1	0.1	581	2.0	13.1	4.8	8.4	5.4	4.0	0.9	35.4	0.78	0.38	66180	3.0	0.25	0.05
FGA87(350)	Pegmatite	63.4	95	4.3	8.9	10458	2.6	15.0	5.3	6.7	75.1	2.2	1.0	18.6	0.63	0.19	2100	12.8	1.58	0.23
FGA53(40)	Pegmatite	463	43	3.3	2.7	45982	6.6	36	2.5	4.1	14.9	1.9	1.9	27.8	0.69	0.02	300	12.8	3.23	0.57
FGA40(140)	Pegmatite	242.8	9	2.5	18.4	20418	2.3	12.5	3	2.6	5.6	0.9	2.1	32.7	0.36	0.02	480	5.7	1.19	0.2

Table 4: Trace element data done by GEOSOL Labs, Belo Horizonte, Brazil.

Sample #	Ba	Be	Ca	Co	Cr	Cu	K	Li	Mg	Mn	Na	Ni	Sb	Sc	Sr	Th	Ti	V	Y	Zn
	ppm	ppm	%	ppm	ppm	ppm	%	ppm	%	%	%	ppm	ppm	ppm	ppm	ppm	%	ppm	ppm	ppm
FGA-03 (20-21)	31	6	1.68	190	62	20	0.04	4	1.5	0.25	0.12	281	18	33	5	<20	4.28	9541	<3	362
FGA-07 (82-83)	5	<3	1.73	296	36	5	<0,01	4	8.49	0.37	0.02	608	<10	27	<3	<20	1.52	3884	<3	171
FGA-14 (40-41)	7	6	0.25	277	36	154	0.01	<3	3.13	0.2	0.01	473	14	31	<3	<20	4.57	>10000	<3	241
FGA-20 (07-08)	22	5	0.88	255	79	28	0.03	<3	1.37	0.17	0.05	491	15	34	5	<20	3.94	>10000	<3	250
FGA-14 (49-50)	9	5	0.36	274	60	29	0.29	4	4.48	0.22	0.02	634	17	25	<3	<20	4.15	>10000	<3	268
FGA-17 (82-83)	6	6	0.52	253	31	20	<0,01	<3	4.57	0.23	0.01	547	18	21	<3	<20	4.36	>10000	<3	253
FGA-20 (20-21)	6	6	<0,01	145	<3	165	<0,01	<3	0.67	0.16	<0,01	249	18	24	<3	<20	4.95	>10000	<3	234
FGA-23 (29-30)	12	5	0.55	255	31	62	0.01	<3	2.03	0.19	0.04	353	14	26	4	<20	4.32	>10000	<3	197

FGA-17 (27-28)	17	7	0.26	157	<3	49	<0,01	4	1	0.17	0.12	276	16	28	4	<20	5.22	>10000	<3	124
FGA-19 (16-18)	41	4	0.65	338	207	27	<0,01	<3	1.98	0.24	0.1	762	14	27	6	<20	3.48	8068	<3	301
FGA-40 (98-100)	18	<3	4.75	190	23	37	0.17	11	4.2	0.2	0.59	268	<10	39	34	<20	1.69	4285	7	111
FGA-58 (85-86)	<3	6	0.06	282	39	94	<0,01	4	2.27	0.2	0.06	501	24	20	<3	<20	5.36	>10000	<3	230
FGA-58 (140-141)	8	5	1.33	248	<3	46	0.05	<3	2.84	0.21	0.05	367	16	27	<3	<20	4.56	>10000	<3	261
FGA-61 (76-77)	184	3	2.98	165	58	16	0.91	45	2.44	0.16	0.53	352	16	27	46	<20	3.12	8062	<3	150
FGA-69 (45-46)	59	4	1.65	208	26	20	0.6	88	2.59	0.14	0.28	457	16	27	15	<20	3.57	>10000	<3	192
FGA-80 (23-24)	287	3	6.1	89	193	343	0.65	20	2.49	0.21	1.3	90	14	48	127	<20	2.6	2079	15	224